JOURNAL OF GEOPHYSICAL RESEARCH, VOL. 97, NO. E5, PAGES 7735–7757, MAY 25, 1992

Atmosphere and Climate Studies of Mars Using the Mars Observer Pressure Modulator Infrared Radiometer

D. J. McCleese,[1] R. D. Haskins,[1] J. T. Schofield,[1] R. W. Zurek,[1] C. B. Leovy,[2] D. A. Paige,[3] and F. W. Taylor[4]

Studies of the climate and atmosphere of Mars are limited at present by a lack of meteorological data having systematic global coverage with good horizontal and vertical resolution. The Mars Observer spacecraft in a low, nearly circular, polar orbit will provide an excellent platform for acquiring the data needed to advance significantly our understanding of the Martian atmosphere and its remarkable variability. The Mars Observer pressure modulator infrared radiometer (PMIRR) is a nine-channel limb and nadir scanning atmospheric sounder which will observe the atmosphere of Mars globally from 0 to 80 km for a full Martian year. PMIRR employs narrow-band radiometric channels and two pressure modulation cells to measure atmospheric and surface emission in the thermal infrared; a visible channel (0.39–4.7 μm) is used to measure solar radiation reflected from the atmosphere and surface. Vertical profiles of atmospheric temperature, the infrared extinction of dust suspended in the atmosphere, atmospheric water vapor, and condensate hazes will be retrieved from infrared measurements having a vertical resolution of 5 km, which is half an atmospheric scale height. PMIRR infrared and visible measurements will be combined to determine the radiative balance of the polar regions, where a sizeable fraction of the global atmospheric mass annually condenses onto and sublimes from the surface. Derived meteorological fields, including diabatic heating and cooling and the vertical variation of horizontal winds, will be computed from the globally mapped fields retrieved from PMIRR data. Analyses of these observed and derived fields will address many key questions regarding the atmosphere and climate of Mars.

1. Introduction

The study of the atmosphere and climate of Mars requires a comprehensive investigation of atmospheric and surface phenomena linked by the physical mechanisms of atmospheric transport, surface-atmosphere interaction, radiative heating and cooling, and latent heat exchange. To date, such studies have been severely limited by the lack of simultaneous and systematic measurements of the distributions of dust, volatiles, and key meteorological fields. Previous missions, beginning with the flyby of Mariner 4 in 1965 and continuing through the more recent Viking and Phobos missions, have been constrained by their limited lifetimes or by the natural limitations of the spacecraft and instrument capabilities available at the time.

The Mars Observer mission will take the next step in the exploration of Mars. In its polar near-circular orbit the spacecraft will be ideally suited to global synoptic mapping of atmospheric constituents and fields. Two of its primary mission goals address the atmosphere and its interactions with the surface; these are to (1) determine the structure of the atmosphere and aspects of its circulation and (2) determine the time and space distribution, abundance, sources, and sinks of volatile material and dust over a seasonal cycle.

Within the Mars Observer instrument payload, the pressure modulator infrared radiometer (PMIRR) is unique in that it is dedicated to observing atmospheric fields globally and nearly continuously in the lower and middle atmosphere of Mars. PMIRR is a nine-channel limb and nadir scanning atmospheric sounder designed to provide measurements of atmospheric temperature, dust, water vapor, and condensate clouds and of surface radiative balance. More specifically, its measurement objectives are to (1) map the three-dimensional and time-varying thermal structure of the atmosphere from the surface to 80 km altitude, (2) map the atmospheric dust loading and its global, vertical, and temporal variation, (3) map the seasonal and spatial variation of the vertical distribution of atmospheric water vapor in the lower atmosphere ($\leq$30 km), (4) identify condensates of H_2O and CO_2 in the atmosphere and map their spatial and temporal variation, (5) measure atmospheric pressure for use as a vertical coordinate and to monitor the seasonal and spatial variation of surface pressure, (6) monitor the radiative balance of the polar regions, and (7) derive surface temperatures, albedo, and thermal inertia.

The combination of systematic viewing of the atmosphere, the relatively high vertical resolution provided by limb sounding, the simultaneous, colocated measurement of temperature, dust, and water vapor, and the synergisms with other Mars Observer instruments will enable the PMIRR investigation to extend significantly our present understanding of the atmosphere and climate of Mars.

The specific scientific objectives of the PMIRR investigation are addressed in section 2. The existing state of knowledge and the outstanding scientific questions related to the atmosphere and climate of Mars are also discussed, together with statements of key measurements to be made and of quantities to be derived from PMIRR measurements. The instrument itself, including calibration procedures, and the instrument observing strategy using to obtain a representative climatology are described in section 3. An outline of the retrieval approach to be used and some numerical simula-

[1]Earth and Space Sciences Division, Jet Propulsion Laboratory, California Institute of Technology, Pasadena.
[2]Department of Atmospheric Sciences, University of Washington, Seattle.
[3]Department of Earth and Space Sciences, University of California, Los Angeles.
[4]Department of Atmospheric, Oceanic and Planetary Physics, Oxford University, Oxford, England.

Paper number 92JE00539.
0148-0227/92/92JE-00539$05.00

tions of the ability of PMIRR to achieve its measurement objectives are presented in section 4.

2. Scientific Objectives

2.1. *Atmospheric Thermal Structure and General Circulation*

Previous measurements, analyses, and modeling studies have identified several of the major components of the general circulation of the atmosphere of Mars (see the reviews by *Leovy* [1985] and *Zurek et al.* [1992]). These include the meridional flow due to the seasonal condensation and sublimation of CO_2 in the polar regions [*Hess et al.*, 1980; *James and North*, 1982], the seasonally dependent zonally symmetric mass transport in the meridional plane [*Leovy and Mintz*, 1969; *Leovy et al.*, 1973; *Haberle et al.*, 1982], traveling and stationary planetary waves in the northern hemisphere [*Pollack et al.*, 1981; *Barnes*, 1980, 1981, 1990*a*], atmospheric thermal tides [*Pirraglia and Conrath*, 1974; *Zurek*, 1976; *Zurek and Leovy*, 1981], internal gravity waves [*Pirraglia*, 1976; *Barnes*, 1990*b*], regional slope winds, dust devils [*Ryan*, 1964; *Ryan and Lucich*, 1983; *Thomas and Gierasch*, 1985], local dust storms [*Gifford*, 1964; *Martin and Baum*, 1969; *Peterfreund*, 1985], and episodically, regional and even planetary-scale dust storms [*Gierasch*, 1974; *Martin*, 1974*a*, *b*, 1976; *Pollack et al.*, 1979; *Zurek*, 1982].

On Mars, dust suspended in the atmosphere can modify the atmospheric thermal structure and various components of the atmospheric circulation to a degree that is quite remarkable by comparison with Earth [*Gierasch and Goody*, 1972; *Hanel et al.*, 1972; *Conrath et al.*, 1973; *Moriyama*, 1976; *Haberle et al.*, 1982; *Zurek et al.*, 1992]. The nonlinear feedbacks involving the transport of dust and the diabatic heating by airborne dust underlie much of the complexity apparent in seasonal and interannual variations of the atmosphere of Mars. Other remarkable features of the planet that are important to its general circulation are the condensation and sublimation of a sizeable fraction of its total atmospheric mass and the presence of its substantial topographic relief. Furthermore, while Mars does not have continents in the sense of a land-sea distribution, there are vast coherent regions of the planet with high surface albedo and low apparent thermal inertia [*Palluconi and Kieffer*, 1981]. These "thermal continents" may have significant effects on the atmospheric general circulation [*Zurek and Christensen*, 1990].

Existing data lack the spatial and temporal coverage of the Martian atmosphere needed to define the full range of its variability and to relate quantitatively possible radiative and mechanical forcing to observed features. The key objectives of the PMIRR investigation in the study of the general circulation of Mars are, first, to describe the time-space structure of the circulation; second, to understand quantitatively the relationship between general circulation features and radiative forcing, as influenced by such factors as atmospheric mass, surface thermal properties, and topography; and third, to constrain quantitatively wherever possible, the role of the general circulation in atmospheric transports and climate change.

PMIRR will characterize large-scale atmospheric variability by repeated scanning of the atmospheric limb of Mars on each of 12-13 orbits per day to provide global, daily views of atmospheric temperatures and dust, both from 0 to 80 km, but using pressure as a vertical coordinate. Although winds cannot be observed directly by PMIRR, the vertical variation of the horizontal wind components (i.e., the wind shear) is related to the horizontal variation of temperature and can be derived from the global mapping of temperature on pressure surfaces.

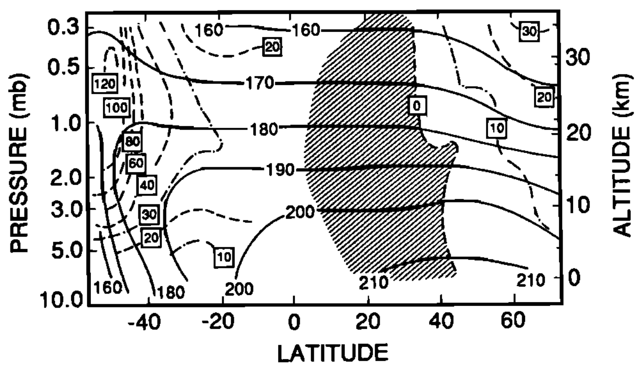

Fig. 1. Latitude-pressure cross section of temperatures (in degrees Kelvin; solid curves) retrieved from Mariner 9 IRIS data for the middle of northern spring (areocentric longitude L_S = 43°–54°). Zonal winds (in meters per second; dashed and dot-dash curves) were computed assuming geostrophic balance and no wind at the surface. The shaded region with the undefined equatorial boundary indicates a region of easterlies (i.e., westward wind); elsewhere, westerlies prevail. (Figure is from *Leovy* [1982] from data provided by B. Conrath.)

Deriving winds from temperatures. The only direct measurements of atmospheric winds on Mars are those made by the two Viking landers at a single height of 1.6 m. Presently, there are no plans to fly instruments that would measure Martian winds directly from orbit, although such instruments are now observing Earth's upper atmosphere [*Reber*, 1990]. Fortunately, the vertical variation of the horizontal wind components (i.e., the wind shears) can be computed from PMIRR's observations of global temperature fields by using the geostrophic or higher-order approximations [*Zurek et al.*, 1992]. Determination of the winds themselves depends upon a boundary condition, such as the precise measurement of surface pressure or the knowledge of the wind at some known height. The required precision in the measurement of surface pressure is difficult to achieve by passive remote sounding from orbit. Cloud tracking by the Mars Observer camera (MOC) can provide the required reference-level winds on those occasions where there are identifiable cloud features which can be located in altitude and tracked from one orbit to the next. This is most likely to occur at high latitudes.

The magnitude of the zonal and meridianal wind components, u and v respectively, at high altitude on Mars (say, above 20 km) is determined largely by the wind shear, since winds near the surface are expected to be small by comparison. For these altitudes it is adequate to assume that $u \approx v \approx 0$ near the surface. Figure 1 shows a meridional cross section of temperature constructed from Mariner 9 infrared interferometer spectrometer (IRIS) data, together with the zonal wind computed using the geostrophic assumption. Unlike the case for Mariner 9, Mars Observer with PMIRR can obtain such cross sections daily for each of 12-13 orbits spanning the planet and with corresponding maps of dust opacity, haze distribution, and water vapor.

Zonally symmetric components of the circulation. The variations of the zonally averaged temperature and zonal mean wind velocity with pressure, latitude, and season constitute two of the most important characteristics of a planet's general circulation [e.g., *Lorenz*, 1967]. They are first-order dynamical properties against which dynamical models, including general circulation models (GCMs), must be validated. PMIRR will provide zonally averaged temperatures at altitudes below 80 km for a full Mars year. Previous latitude-height cross sections of the zonal mean temperatures have been confined to altitudes below 45 km and largely during northern spring [*Leovy*, 1982].

The region above 45 km is of particular interest in that it is virtually unexplored. There is some evidence [*Deming et al.*, 1986] that, just as in the case of the Earth's mesosphere, the latitudinal variation of temperature may be far from the radiative equilibrium distribution. Observation of such departures from equilibrium over seasonal time scales would provide clear evidence that the breaking of vertically propagating gravity waves and atmospheric tides is playing a significant role in the momentum balance of the middle atmospheres of both Earth and Mars. The effective "drag" exerted on the zonal mean Martian circulation by these breaking waves can be estimated from temperature observations, just as for Earth [*Smith and Lyjak*, 1985].

The zonal mean component of the zonal wind can be computed in a rather straightforward way from the observed temperature field, as discussed above (see Figure 1). The zonally averaged meridional wind cannot be estimated in this fashion, since the zonal average of the longitudinal pressure gradient is zero; thus the zonal mean component of the meridional wind results from a complex interplay of pressure forces and wave-induced fluxes of heat and momentum. Yet, a thermally driven Hadley-type circulation on Mars, with its zonal mean meridional wind, may be an effective means of transporting dust and volatiles across the planet [e.g., *Haberle et al.*, 1982; *Zurek et al.*, 1992]. Theory and numerical simulation indicate that the intensity of a cross-equatorial Hadley circulation on Mars and its meridional extent are closely tied to the opacity and to the vertical and horizontal extent of dust hazes in the atmosphere. The intensification and poleward extension of this circulation is likely to be greatest during the episodic planet-encircling dust storms [e.g., *Haberle et al.*, 1982; *Zurek et al.*, 1992].

One signature of the Mars Hadley circulation during a great dust storm is the reversal aloft of the poleward temperature gradient due to adiabatic warming in the downwelling branch of the circulation. The position of this relatively warm air will move with latitude as the amount of dust and the area covered by dust changes with time. PMIRR has the spatial resolution and coverage to identify these variations in the upper layers of the dust haze.

By combining the thermodynamic energy and mass continuity equations the zonal mean meridional and vertical winds can each be represented as the sum of two components, one related to the diabatic heating of the atmosphere and the other to the meridional flux of heat due to atmospheric waves. The wave-induced component is difficult to estimate from Mars Observer data, in part because of the difficulty discussed earlier of computing winds as opposed to wind shears. However, theory and terrestrial experience indicate that the zonally averaged transport due to advection by the diabatically driven component of the zonal mean meridional and vertical winds is a good approximation to the net zonal mean transport, which is the difference between advection by the zonally averaged winds and the zonal mean component of meridional fluxes induced by planetary waves. The diabatically related zonal mean meridional and vertical velocities are therefore referred to as the residual zonal mean circulation [*Andrews et al.*, 1987].

Derivation of residual zonal mean circulations has proved useful for the study of the transports of ozone, water vapor, and other trace species in the Earth's stratosphere [*Garcia and Solomon*, 1983; *Gille et al.*, 1987]. For Mars the residual mean circulation can be estimated from PMIRR data, using observed temperatures and a computed diabatic heating which depends primarily on the distribution of atmospheric dust.

Wave components of the general circulation. Observationally, atmospheric waves are the longitudinally varying components of the meteorological fields. Such waves are characterized by a vast range of spatial and temporal scales. Four important categories of large-scale waves are discussed here.

Traveling planetary waves: The two Viking lander meteorology stations detected traveling waves during winter at both the 23°N and 48°N sites, with the wave activity more prominent and more frequent at the more poleward site. With the aid of the geostrophic approximation these waves were inferred to be typically of zonal wavenumber 3 or 4 with eastward phase speeds in the range 10–20 m/s. On this basis they have been tentatively attributed to baroclinic instability [*Barnes*, 1980, 1981]. The location and character of these waves were observed to vary with atmospheric dust loading. Occasionally, the waves themselves appeared to trigger local dust storms [*Briggs and Leovy*, 1974; *Ryan et al.*, 1981; *Arvidson et al.*, 1983].

Planetary-scale waves were also detected in the Mariner 9 IRIS observations, but orbital geometry precluded the unambiguous determination of both zonal wavenumber and period [*Conrath*, 1981]. It is not known if wintertime wave disturbances occur in the mid-latitudes of the southern hemisphere. Simulations using GCMs of the atmosphere of Mars suggest that the occurrence of these waves in the southern mid-latitudes is highly sensitive to the uncertain features of the large-scale topography there (J. R. Barnes et al., private communication, 1991).

Stationary waves: Inferences based on Mariner 9 IRIS data [*Conrath*, 1981] and simulations using a variety of atmospheric circulation models indicate that the large-amplitude planetary-scale orography and variation in surface properties [*Webster*, 1977; *Moriyama and Iwashima*, 1980; *Pollack et al.*, 1981] will drive a strong atmospheric response. The long-period traveling component of this response was discussed above. Model simulations suggest that the stationary, or quasi-stationary (periods > 10 days or so), response may be even larger. The nature of this response is thought to take the form of vertically propagating Kelvin waves at low latitudes and of vertically trapped Rossby waves at higher latitudes [*Webster*, 1977]. The theory of these disturbances is well developed, and abundant observations of these phenomena exist for Earth's atmosphere. On Mars, amplification of orographically forced waves during planetary-scale dust storms can provide a very effective means of transporting heat and dust into the polar regions [*Barnes and Hollingsworth*, 1987].

PMIRR observations have sufficient spatial resolution to reveal unambiguously the characteristic zonal wavenumbers, phase speeds, vertical scales and meridional extent of stationary and of most traveling planetary-scale waves (see section 3). Observations of the wintertime southern hemisphere will establish whether or not traveling waves occur in the south, as they are known to do in the north. The Mars Observer laser altimeter (MOLA) will define planetary-scale as well as smaller-scale components of the terrain height. This will provide a critical test of hypotheses about the influence of topography on traveling waves. PMIRR observations of the variations of the dust distribution and of temperature will also link quantitatively the effects of net radiative forcing by suspended dust to the modification or generation of atmospheric waves.

Atmospheric tides: On Mars, planetary-scale oscillations of the meteorological fields known as atmospheric tides are driven principally by the daily varying solar heating of the atmosphere and surface [*Zurek*, 1976]. Observations of surface pressure and winds by the Viking landers [*Leovy*, 1981], together with atmospheric temperature observations by the Mariner 9 IRIS [*Pirraglia and Conrath*, 1974], the Viking lander entry science package [*Seiff and Kirk*, 1977], and the Viking infrared thermal mapper (IRTM) [*Martin*, 1981], show that atmospheric tides are a significant component of the general circulation, particularly during planetary-scale dust storms [*Zurek and Leovy*, 1981].

The largest components of the diurnal (i.e., once daily) and semidiurnal (i.e., twice daily) tidal fields are fixed in local time, but the large-amplitude planetary-scale orography of Mars and the presence of its "thermal continents" may induce components which are not locked to the Sun's apparent motion. One eastward traveling tidal component of particular interest is an apparent diurnal Kelvin mode [*Zurek*, 1976; *Conrath*, 1976], which may be greatly amplified during the early stages of a great dust storm and thereby provide a positive feedback leading to more dust raising [*Zurek and Leovy*, 1981; *Tillman*, 1988].

In its nominal observational mode, PMIRR will characterize diurnal atmospheric tides using the day-night (1400-0200 Mars LT) differences in the temperatures observed on constant pressure surfaces. This approach has been utilized in the study of tides in Earth's stratosphere [*Hitchman and Leovy*, 1985]. The nominal observations will be supplemented on occasion by viewing local time differences of about 3 hours using the ability of PMIRR to look in the cross-track direction at the atmosphere at both side limbs (section 3.5).

Some tidal components will grow in amplitude with height, especially at low latitudes, and these will be readily observed by PMIRR in the middle atmosphere. The vertical structure of the waves above 30 km will also permit the identification of the heights of tidal breaking, a process which may drive mechanically the circulation of the Mars middle atmosphere through turbulent mixing and momentum dissipation [*Zurek*, 1986].

Free modes: In contrast to the thermally driven atmospheric tides discussed above, atmospheric free modes rise above the meteorological noise because of the resonant properties of the global waveguide provided by the background temperature structure. The Viking lander surface pressure record suggests that free modes are present, and it has been suggested that they may play a role in "triggering" large-scale dust storms [*Tillman*, 1988].

On Mars the frequencies of these resonant modes are close to the diurnal and semidiurnal harmonic frequencies of the thermally forced tides [*Hamilton and Garcia*, 1986; *Zurek*, 1976, 1988]. PMIRR data will be used to isolate modes of nearly diurnal frequency; the data will also provide simultaneous information on the background temperatures which determine the frequencies of the resonant, or free-mode, response through the formation of the atmospheric waveguide.

2.2. *Dust in the Atmosphere*

Radiative effects of airborne dust. Dust suspended in the atmosphere of Mars absorbs and scatters incoming solar radiation; at the same time it absorbs and reemits thermal radiation from the surface. In so doing, suspended dust greatly affects atmospheric heating [*Gierasch and Goody*, 1972; *Moriyama*, 1976; *Zurek*, 1978; *Pollack et al.*, 1979; *Zurek et al.*, 1992] and modifies the net radiation at the surface [*Davies*, 1979; *Ryan and Henry*, 1979]. The key parameters determining the radiative effects of dust suspended in the atmosphere are, first, the spatial distribution of the dust and its variation with time and, second, the optical properties of the dust, including the visible and infrared opacities and the effective single-scattering albedo and phase function of the dust particles.

The temperatures and infrared extinction by dust retrieved from PMIRR data provide key constraints on the computations of atmospheric heating and cooling due to CO_2 and airborne dust. The ratio of infrared to visible opacity, as well as scattering properties, depend on particle size, shape, and composition [*Kahn et al.*, 1992]. The variation of opacity with wavelength, as observed by PMIRR's mid-IR broadband radiometric channels, provides some constraint on the dust particle size distribution, although more refined estimates of microphysical properties can be derived in combination with the higher spectral resolution data of the thermal emission spectrometer (TES). Estimates of visible opacity are constrained further by the PMIRR wideband solar channel observations, by sequences in which the TES wideband solar channel views the same surface area at multiple emission angles, and by MOC images of the limb and surface.

The dust cycle. The most dramatic component of the seasonal and interannual variation of atmospheric dust is the episodic occurrence of planetary-scale dust storms [*Gierasch*, 1974; *Zurek*, 1982; *Martin*, 1984; *Kahn et al.*, 1992]. Earth-based observations [*Martin*, 1974*a*, *b*; 1976] suggest that such storms originate when one or more localized centers of dust activity expand and coalesce until most of a zonal corridor in the southern hemisphere is obscured. Once the storm encircles the planet, it may expand to other latitudes, including the northern hemisphere. This onset and expansion phase lasts several days and is followed in just a few days by a slow clearing over several weeks and months of the airborne dust [*Conrath*, 1975; *Pollack et al.*, 1979].

Major questions regarding these great dust storms remain unanswered. What are the conditions that lead to the occurrence of one or more such dust storms in some years yet none in others [*Leovy et al.*, 1985; *Haberle*, 1986; *Tillman*, 1988]? The fact that these storms occur most frequently during southern spring and summer, when Mars is closest to the Sun, provides a clue that remains to be deciphered [*Zurek*, 1982]. What causes only a few of the many local dust storms to expand to regional scale? What are the mechanisms controlling the rate of atmospheric clearing, which seems remarkably uniform [*Conrath*, 1975; *Pollack et al.*, 1979]? Model simulations [*Murphy et al.*, 1990] indicate that particle size and shape may play roles, while major influences are exerted by atmospheric mixing and the large-scale circulation.

Major questions remain as to the relative roles in the dust cycle as a whole of various atmospheric circulations, including those driven by the diabatic heating due to the dust itself [*Leovy et al.*, 1973; *Briggs and Leovy*, 1974; *Haberle et al.*, 1982; *Kahn*, 1983; *Arvidson et al.*, 1983; *Barnes*, 1990*a*; *Kahn et al.*, 1992; *Zurek et al.*, 1992]. Locations of the surface sources and sinks of the airborne dust remain uncertain. Once suspended in the atmosphere, dust may be transported into the north polar regions and incorporated into the polar layered terrains [*Pollack et al.*, 1979]. Dust may also be redistributed into those regions of the northern subtropics having high albedo and low thermal inertia [*Christensen*, 1986].

PMIRR addresses these questions in two ways. First, the large-scale thermal structure of the atmosphere will be observed prior to, during, and after the onset of a great dust storm, should one occur during the Mars Observer mission. In addition, the vertical and meridional spreading and subsequent clearing of the dust hazes will be mapped with good spatial and temporal resolution. This will permit the estimation of the radiative forcing and the monitoring of changes in (1) the background atmospheric static stability, (2) the residual mean circulations, and (3) large-scale stationary and traveling waves, including atmospheric tides. In this manner the PMIRR data should illuminate the radiative-dynamical mechanisms involved in the generation and dissipation of the planetary-scale dust storms on Mars.

2.3. *The Water Cycle*

Much of the past and present interest in the climate of Mars stems from speculation on existence and behavior of water on its surface and in its atmosphere. Water in the current epoch is characterized by a few to several tens of precipitable microns (pr μm) of vapor in the atmosphere and by a permanent water ice polar cap in the north which is the only known surface reservoir. Other possible reservoirs are, in likely order of importance to the atmosphere, water vapor adsorbed in the regolith, near-surface ground ice, and the south polar residual CO_2 cap.

Ground-based and spacecraft data, most notably those from the Mariner 9 and Viking missions, have established clear signatures of seasonal variability in the abundance and distribution of atmospheric water vapor [*Hanel et al.*, 1972; *Farmer et al.*, 1977; *Farmer and Doms*, 1979; *Jakosky and Farmer*, 1982; *Jakosky*, 1985; *Haberle and Jakosky*, 1990; *Jakosky and Haberle*, 1992]. Data from the Mars atmospheric water detectors (MAWD) onboard the two Viking orbiters have contributed most to our understanding of the water cycle. MAWD measured column amounts of water over the sunlit portion of the planet for more than a full seasonal cycle (Figure 2). Earth-based observations by *Barker et al.* [1970] and more recent measurements by ground-based infrared and microwave techniques suggest

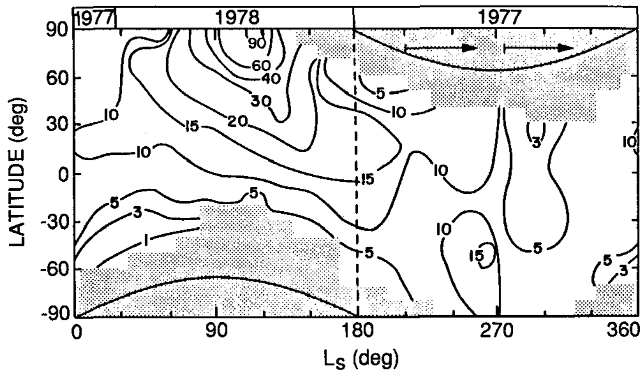

Fig. 2. The seasonal cycle of the zonally averaged vertical column abundance of atmospheric water vapor, as derived from Viking Mars atmospheric water detector measurements for one Mars year. Seasonal date is given in terms of L_S, the areocentric longitude of the Sun; Earth year is indicated at the top. Units are precipitable microns. Stippled regions indicate areas of no data, principally in the polar nights. The two horizontal arrows indicate the periods of onset and dissipation of the two planetary-scale dust storms that occurred during the year. (Figure is adapted from *Jakosky and Farmer* [1982].)

substantial interannual variability in the amount of atmospheric water vapor, particularly in the southern hemisphere [*Jakosky and Barker*, 1984]. Such variability may be related to the annual persistence or disappearance of the south polar residual CO_2 cap [*Kieffer*, 1979; *Jakosky and Haberle*, 1992].

Attempts to use the MAWD, IRTM, and Earth-based observations to estimate quantitatively surface and near-surface sources and sinks of water vapor have thus far met with only limited success. Studies using numerical models of surface-atmosphere exchange and atmospheric circulation [*Davies*, 1981; *Jakosky*, 1983*a*, *b*; *James*, 1985; *Haberle and Jakosky*, 1990] have failed to reproduce the full seasonal variation of the distribution and abundance of atmospheric water that is apparent in the data. One reason for this difficulty is the remaining uncertainty as to whether or not the regolith plays a significant role as a source of water for the atmosphere.

A related problem is the apparent difficulty current models have in transporting enough water from high to low latitudes to duplicate the MAWD observations [*Haberle and Jakosky*, 1990]. Such studies suggest local sources of water at tropical and middle latitudes. However, uncertainties in sublimation and desorption rates and the currently limited knowledge of atmospheric relative humidity and of atmospheric transports severely constrain our ability to describe quantitatively the Mars water cycle.

The PMIRR investigation addresses these uncertainties by simultaneously observing surface temperatures and the vertical profiles of temperature and water vapor abundance and by detecting the presence and location of water ice hazes in the atmosphere. Mapping the vertical variations of water vapor with good resolution should constrain atmospheric transports by cross-equatorial Hadley circulations and by atmospheric waves. Determining the vertical distributions of relative humidity, water ice, and dust hazes can constrain models of the vertical redistribution of water vapor in the atmosphere and of its loss to the surface by condensation and snow [*Kahn*, 1990]. The simultaneous, colocated observation of temperature and water vapor and of the location of dust and ice hazes may provide some constraints on the horizontal transport of water ice, including effects of the nucleation of water ice on suspended dust particles.

2.4. CO_2 Cycle

Carbon dioxide is the dominant constituent of the Martian atmosphere and the most volatile and dynamic component of the Mars climate system. A full understanding of the Martian climate requires determination of the sizes of surface and subsurface reservoirs of condensed CO_2 and their behavior over seasonal and climatic time scales, as well as understanding the seasonal and long-term interactions between the CO_2, dust, and water cycles. Existing spacecraft and ground-based observations have provided us with a good first-order picture of the present seasonal CO_2 cycle [*Paige*, 1985; *Paige and Ingersoll*, 1985; *James et al.*, 1992], but to extend this understanding to interannual time scales and beyond will require a considerably more detailed understanding of the properties and processes that are responsible for the presently observable behavior.

Reservoirs of CO_2 identified in earlier observations include (1) the atmosphere with ~14 g/cm^2 of CO_2 averaged over the globe, (2) the seasonal polar caps which contain 0–3 g/cm^2 of CO_2 averaged over the globe, and (3) a residual CO_2 frost deposit near the south pole [*Kieffer*, 1979; *Paige et al.*, 1990], which has been estimated to contain less than 14 g/cm^2 of CO_2 averaged over the globe [*Fanale*, 1976] and which may disappear completely in some years. Additional reservoirs which may be significant include adsorbed CO_2 in the Martian regolith [*Fanale and Cannon*, 1979] and carbonates [*Pollack*, 1979; *Kahn*, 1985; *Pollack et al.*, 1987]. Potentially, either of these reservoirs may contain significantly more volatile carbon than is presently observed in the atmosphere and polar caps.

Models for the behavior of Martian CO_2 over seasonal and climatic time scales indicate that in equilibrium the partitioning of exchangeable CO_2 between the gas and the condensed phases is governed primarily by temperature. When a permanent CO_2 cap is present, the mass of CO_2 gas in the Martian atmosphere is determined by the vapor pressures of the permanent frost deposits, as determined by their annual averaged temperatures [*Leighton and Murray*, 1966]. When a permanent CO_2 cap is not present, the mass of the Martian atmosphere could be determined by the vapor pressures of adsorbed CO_2 deposits, which are strongly temperature dependent [*Fanale and Cannon*, 1979] or by the formation of carbonates, which are formed most rapidly when atmospheric temperatures permit the presence of liquid water, possibly in disequilibrium [*Kahn*, 1985].

The recession and growth of the Martian seasonal polar caps are governed largely by their heat balance. The Viking IRTM observations provided the first direct measurements of the most important heat budget quantities over an annual cycle for the north and south polar residual caps [*Paige*, 1985; *Paige and Ingersoll*, 1985]. PMIRR has a wideband solar channel and several radiometric filter channels in the thermal infrared to measure reflected solar and thermal radiation emerging from the top of the Martian atmosphere. The PMIRR observations of the polar heat balance will go beyond the Viking data by (1) providing a more systematic and accurate set of heat balance measurements over wider geographic regions at high northern and southern latitudes and (2) making simultaneous measurements of polar surface temperatures and of atmospheric fields necessary to constrain quantitatively individual terms in the heat balance of the polar surface and atmosphere.

The major term in the heat balance is the net radiative gain of the atmosphere-surface system and is computed from PMIRR data using the measured broadband visible and several infrared radiances. Smaller terms include (1) rates of subsurface heat conduction, determined through measurements of bare ground and water ice surface temperature variations, (2) atmospheric heat storage, determined by measurements of polar atmospheric temperatures, and (3) net atmospheric heat transport, constrained through measurements of global temperature and aerosol fields combined with computed estimates of atmospheric winds or with dynamical models. The computation of these terms, together with observations by PMIRR of dust and ice hazes at high latitudes and of surface and atmospheric fields at lower latitudes, will form a basis for a better understanding of the present seasonal CO_2 cycle on Mars and the factors controlling it, including its interaction with the cycles of water and dust.

2.5. Surface Science

Characterizing the physical and chemical properties of the surface of Mars is one of the principal scientific goals of the Mars Observer mission. Images of the surface of Mars show evidence for a wide range of surface modification processes, some undoubtedly atmospheric in origin, that have operated over Mars' history and have helped to shape the Martian terrain. Surface temperatures are a key diagnostic of properties and processes connecting the atmosphere and surface on diurnal and seasonal time scales. Surface temperatures represent important boundary conditions for considerations of the thermal and dynamic state of the atmosphere, the physical and chemical properties of the surface and subsurface, and the distribution of ground ice and other volatiles.

Under present climatic conditions, Martian surface temperatures are affected by a wide range of atmospheric processes including (1) scattering and absorption of incident solar radiation by aerosols and gases, (2) scattering, absorption, and emission of infrared radiation by aerosols and gases, and (3) conductive and convective heat transfer between surface and atmosphere in the planetary boundary layer. Therefore surface temperatures are determined not only by the physical properties of the surface itself but by net effects of the atmosphere on the surface heat balance [*Haberle and Jakosky*, 1991].

Efforts to understand the present thermal state of the Martian surface and its diurnal and seasonal variability have been severely hampered by a lack of detailed, simultaneous atmospheric observations. PMIRR will rectify this deficiency by routinely retrieving accurate surface temperatures over wide geographic regions with simultaneous determinations of atmospheric temperatures, dust loading, and the combined reflectivity of the surface-atmosphere system. These observations will be used in conjunction with models of the heat balance of the surface-atmosphere column from which key surface parameters, such as thermal inertia and albedo, and the net effect of the atmosphere on the surface heat balance will be derived. Determining these parameters will provide, among other things, improved global-scale constraints on the size distributions of Martian surface materials and aeolian deposits.

3. Measurement Approach and Instrument Description

Confidence in the ability of PMIRR to achieve the necessary measurement objectives is based in part on numerical simulations (see section 4) and in part on its heritage. The observational study of Earth's stratosphere over the past 25 years serves as a paradigm for the investigation of the atmosphere of Mars, a regime of comparable pressures, temperatures, and water vapor abundances. Detailed observations of Earth's middle atmosphere have been and are now largely performed by limb viewing experiments because of the need to achieve vertical resolutions better than one atmospheric scale height.

The utility of high vertical resolution profiles has been demonstrated for Earth by the scientific impact of data from the limb infrared monitor of the stratosphere (LIMS [*Gille and Russell*, 1984]) and the stratospheric and mesospheric sounder (SAMS [*Barnett et al.*, 1985]) onboard the Nimbus 7 satellite. In the fall of 1991 a new generation of limb sounders deployed on the Upper Atmosphere Research Satellite (UARS [see *Reber*, 1990]) began to map the global distributions of temperature and minor constituents in Earth's middle atmosphere. These instruments, several employing infrared filter and gas correlation spectroradiometry, achieve vertical resolutions of half an atmospheric scale height or better.

As for Earth, the characteristic thermal structures in the Mars atmosphere have vertical scales of 1–2 atmospheric scales [e.g., *Seiff and Kirk*, 1977; *Leovy*, 1985; *Barnes*, 1986]. In addition, Mars presents the difficulty that dust is often suspended in its atmosphere [e.g., *Pollack et al.*, 1979], and so its contribution to the observed radiance must be separated from that due to thermal emission by CO_2 or H_2O gas. Thus the design of PMIRR and its observational strategy are driven by the need to (1) retrieve atmospheric fields with adequate vertical resolution, (2) retrieve vertical profiles of temperature and water vapor in the presence of aerosols and retrieve simultaneously the vertical profile of aerosol extinction, and (3) quantify the radiative fluxes of the polar regions. To achieve these goals, PMIRR has adapted to the global mapping of Martian atmospheric properties the techniques of limb sounding and filter and pressure modulation radiometry proven for the study of Earth's stratosphere.

3.1. *Instrument Specifications*

An early, detailed description of the PMIRR instrument design was published by *McCleese et al.* [1986]. The completed instrument is shown in Figure 3. Table 1 summarizes the band pass, type, and measurement function of the PMIRR spectral channels, while the chief physical and operational parameters of the instrument are given in Table 2. Briefly, PMIRR observes in a broadband visible channel and in eight spectral intervals in the 6- to 50-μm range. Spectral discrimination within this infrared range is achieved using spectral filters and pressure modulator units. An adequate signal-to-noise ratio in the temperature and water vapor sounding channels 1–4 is ensured through the placement of their detectors on a cold focal plane assembly cooled to 80 K by a passive radiative cooler. Vertical profiles of atmospheric properties are constructed from observations in three fields of view (FOV) scanned across the limb and onto the planet using a two-axis scan mirror in front of the primary telescope.

Optics. The PMIRR optical layout is shown schematically in Figure 4. All channels share a common scan mirror and telescope primary, and all channels view Mars and space alternately at 800 Hz via a rotating double-sided mirror chopper. The CO_2 and H_2O pressure modulator cells (PMCs) are located in the optical paths of channels 1–4 and impress a 50-Hz amplitude modulation on to the chopped signal.

Optical mechanisms. The key PMIRR optical mechanisms are the pressure modulator units (PMUs), the scan mirror assembly, and the chopper assembly. The PMUs mechanically modulate the pressure of gas within a sealed optical cell, using dynamically balanced pistons driven at resonance [*Taylor*, 1983]. The scan mirror assembly, consisting of elevation and azimuth drive actuators mounted orthogonally in a yoke arrangement, allow the mirror orientation to be stepped over a large angular range in both axes. The chopper assembly is a rotating disc with 12 teeth, driven at 4000 rpm, which provides continuous and full (100%) signal modulation at 800 Hz.

Detectors. The nine PMIRR channels employ single element detectors. Channels 1–5 use cooled HgCdTe photon detectors, whereas channels 6–9 use ambient temperature deuterated triglycine sulfate (DTGS) pyroelectric detectors. Channels 1 and 4 make use of photovoltaic detector technology, while the channel 2, 3, and 5 detectors are photoconductive. Channels 6 and 7 each have two detectors and hence two FOVs; all others have a single FOV.

Cold focal plane assembly and passive radiative cooler. The PMIRR cold focal plane assembly (CFPA) consists of channel 1–5 detectors, condensing optics, bandpass filters, and their mounting structures cooled by the cold stage of the PMIRR passive radiative cooler and surrounded by concentric housings cooled in turn by the radiator intermediate and warm stages. The three-stage passive radiator has a reclosable door which acts as a planet shield when open and protects cold surfaces from contamination when closed. The mechanical and optical designs of the CFPA are driven by the need to minimize the radiative energy from the 300 K instrument cavity falling on the 80 K focal plane while maximizing the signal throughput in the bandpass of each channel.

Electronics and signal processing. Digital logic control and data processing electronics interface with the spacecraft payload data system, receiving and executing commands and processing instrument science and engineering data. A microprocessor is used for executive control, for example, to implement an automatic PMIRR scan mirror cycle. The primary instrument programs reside in read only memory (ROM) and are copied into random access memory (RAM), where they can be modified through links to changes made in RAM using small-scale memory loads.

While the mechanical chopper produces an 800-Hz signal in all PMIRR channels, the PMUs also produce a 50-Hz sideband signal which appears as an amplitude modulation on the wideband signal. The analog signal processing electronics convert these signals into digital voltage levels. A wideband signal chain amplifies and filters each 800-Hz signal. These signals are then demodulated, filtered, and fed into a voltage-to-frequency converter which is accurately gated into a counter for the signal integration period. The

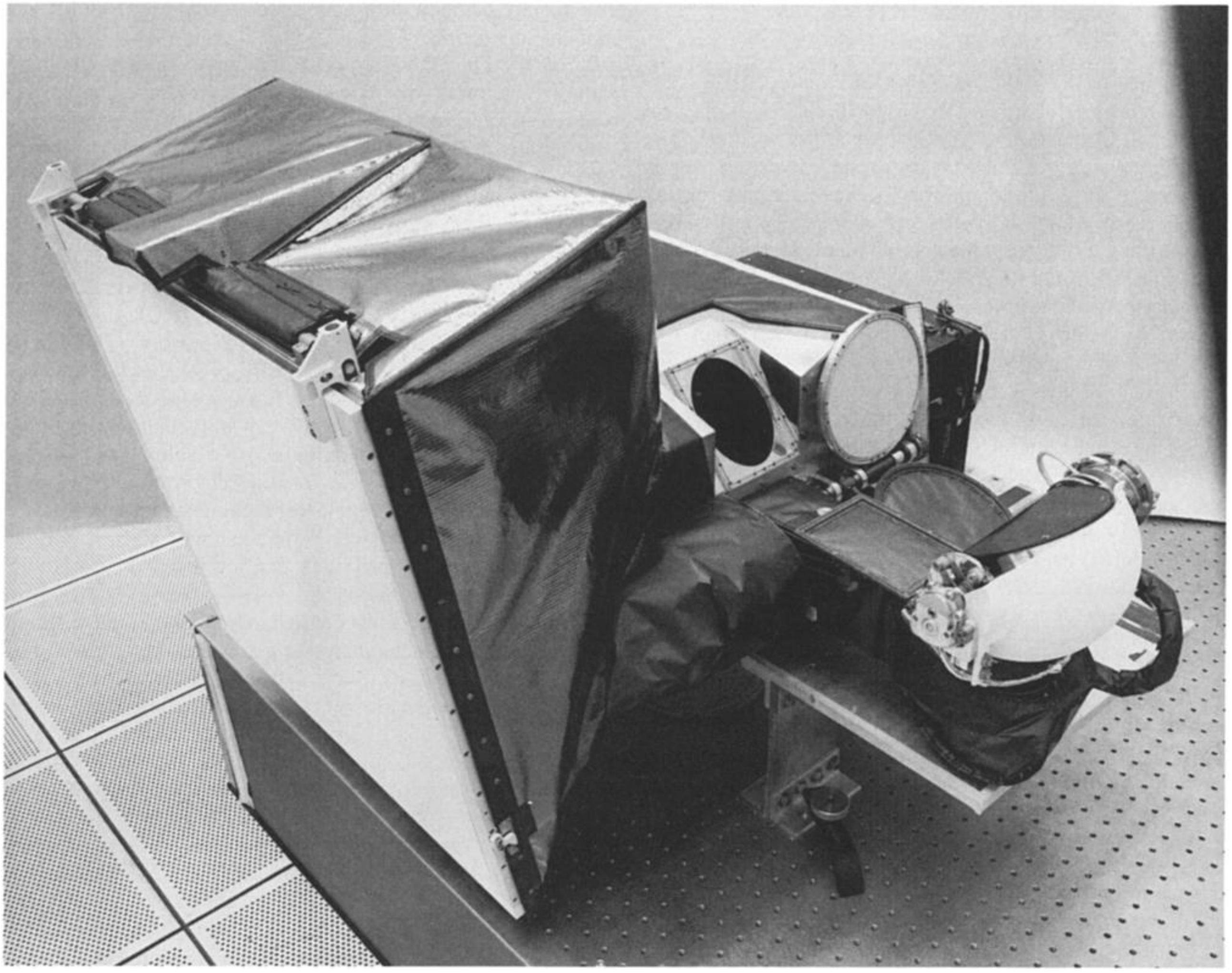

Fig. 3. The pressure modulator infrared radiometer instrument. The scan mirror assembly is in the right foreground, with the dark instrument aperture next to the circular solar calibration target. The deployable covers for the aperture and solar target are also visible. The scan mirror has been rotated into the white hemispherical housing, where it can be stored to avoid damage or contamination. A separate box housing electronics is seen to the right of the solar target. The passive radiative cooler is on the left, with its cover closed. Once in orbit, the cooler door swings outward (and "upward" in this perspective), shielding the radiator from emission from Mars and providing it with a view of space.

sideband signal chain is very similar in function, except that its demodulator reference is taken from the PMU drive waveform rather than the chopper, and its input is the demodulated wideband signal.

Expected instrument performance. Basic figures of merit for a PMIRR channel can be defined as follows.

$$NER = (NEP\ \pi)/(4/\pi A\Omega WF(2\tau)^{1/2}) \quad \mathrm{W\ cm^{-2}\ (sr^{-1}/cm^{-1})},$$

$$S/N = B(\nu_0,\ T_0)/NER,$$

$$NE\Delta T = NER/[dB(\nu_0,\ T_0)/dT] \quad \mathrm{K},$$

$$T_{\min} = B^{-1}(\nu_0,\ NER) \quad \mathrm{K}.$$

where NER is the noise equivalent radiance, or the radiative flux incident on the instrument required to produce an rms signal referenced to the detector equal to the detector noise equivalent power (NEP, W Hz$^{-1/2}$). NER depends only on detector NEP, instrument etendue ($A\Omega$, cm^2 sr^{-1}), equivalent channel spectral width (W, cm^{-1}), channel optical transmission F, and signal integration time (τ, seconds). S/N is the channel signal-to-noise ratio for a view of a blackbody at wavelength ν_0 and temperature T_0, where $B(\nu_0, T_0)$ is the Planck function. $NE\Delta T$ is the noise equivalent temperature change, or the blackbody target temperature change that produces a signal change equal to the noise. Finally, $T_{\min}$ is the minimum detectable temperature, or the blackbody target temperature that gives a signal equal to the noise, where $B^{-1}(\nu_0, NER)$ is the inverse Planck function.

The PMIRR far-IR and visible broadband channels have a detector-noise-limited performance. When observing a blackbody target at a typical Martian temperature of 225 K, channels 6–9 have a $S/N \approx 100$ and an $NE\Delta T \approx 1$ K. The broadband visible channel 9 has a $S/N \approx 3500$ when viewing a normally illuminated, unit albedo surface at the mean Mars distance. The wideband signals for channels 1–5, with their cooled detectors, are digitizer limited. At 225 K, their

TABLE 1. Pressure Modulator Infrared Radiometer Spectral Channels

Channel	Bandpass, cm^{-1}	Central Wavelength, μm	Channel Type*	Nominal Altitude Range, km	Measurement Function†
1	1226–1420	7.6	PMR [CO_2] + WB	0–15	temperature
2	719–739	13.7	PMR [CO_2] + WB	15–50	temperature
3	678–702	14.5	PMR [CO_2] + WB	50–80	temperature
				30–50	pressure
4	1408–1500	6.9	PMR [H_2O] + WB	0–40	water vapor
5	821–873	11.8	WB	20–80	dust, water ice
6	470–506	20.5	WB	0–80	dust, T_S
7	280–334	32.6	WB	0–80	dust, T_S
8	184–230	48.3	WB	0–40	dust, water vapor, T_S, water ice
9	2,116–25,510	0.72	WB	0–40	radiative balance‡, dust properties

*PMR denotes a radiometer channel which passes the incoming radiation through a pressure modulation cell (PMC) containing the identified gas. WB denotes a filter, or wideband, radiometer channel.

†T_S denotes the best channels for deriving surface temperature.

‡Infrared emission is computed for radiative balance studies using all wideband IR channels (i.e., 1–8).

(digitized) S/N performance ranges from 3600 for channel 4 (at 6.9 μm) to 13,000 for channel 3 (at 14.5 μm, closer to the peak blackbody intensity). Corresponding $NE\Delta T$s are 0.006 and 0.003 K.

3.2. *Pressure Modulation Radiometry*

Gas correlation radiometry combines high spectral discrimination and high energy grasp. One implementation of this approach is the pressure modulation technique developed for temperature and species profiling in the terrestrial upper atmosphere [*Taylor*, 1983]. Its principal advantage is that it is species specific. For Mars this means that radiation originating from the ubiquitous airborne dust can be distinguished unambiguously from gaseous emission by atmospheric carbon dioxide and water vapor. This is especially important when limb sounding, as the long atmospheric paths observed heighten sensitivity to suspended dust (see section 3.4).

TABLE 2. Pressure Modulator Infrared Radiometer Instrument Summary

Instrument Parameter	Value
Telescope aperture	
diameter (cm)	6.0
area (cm^2)	28.3
Field-of-view	
detector (deg)	0.19 × 0.95
instrument (deg)	1.70 × 0.95
Etendue ($A\Omega$)	
detector (cm^2 sr)	1.54×10^{-3}
instrument (cm^2 sr)	1.39×10^{-2}
Signal integration envelope (s)	2
Data rate	
science (bps)	120
housekeeping (bps)	36
Mass (kg)	44.1
Power	
mean (W)	36.5
peak (W)	37.5
Dimensions	
instrument (cm)	30 × 23 × 74
cooler (cm)	58 × 65 × 30
electronics (cm)	13 × 20 × 33

A PMIRR pressure modulator radiometer (PMR) channel is shown schematically in Figure 5. A PMR allows detection of radiation from the emission lines of a specific atmospheric gas by directing atmospheric emission through an optical cell containing the same gas. For PMIRR, opacity variations of CO_2 or H_2O in the optical path of the channel are produced by modulating gas pressure in an optical cell (Figure 5) using pistons driven near their resonant frequency (≈50 Hz). Mean pressure is maintained by a temperature-controlled molecular sieve reservoir.

Because the transmission of the pressure modulator cell (PMC) varies at the frequency of modulation only near gaseous absorption lines, the pressure modulated signal quantifies atmospheric emission in spectral regions in and near the absorption lines in the PMC, which match the emission lines of the same gas in the atmosphere. The chopped, or wideband, signal provides a measure of uncorrelated scene radiation while largely rejecting atmospheric emission from the gas of interest.

Figure 6 illustrates the spectral discrimination of a PMR for a single CO_2 line in a limb view of the Martian atmosphere. The curves labeled T_{p1} and T_{p2} show the transmission of the PMC at the two extremes of the modulator pressure cycle, and the curve labeled $T_{p1} - T_{p2}$ is the effective transmission at the modulation frequency. The spectral resolution of a PMR is determined primarily by cell length and the mean pressure of the gas in the cell and can be designed to match atmospheric emission line profiles (Figure 6). Because a PMR channel is defined by a broad bandpass filter, 50–100 emission lines can be observed simultaneously giving the PMR a multiplex advantage [*Houghton and Smith*, 1970].

3.3. *Instrument Calibration*

Calibration is the process that allows the relationship between the radiance incident on the instrument in each spectral channel and the digital data output from that channel to be determined. PMIRR radiance measurements are made in spectral channels that cover a wide spectral range, and accurate calibration is possible only if the radiometric,

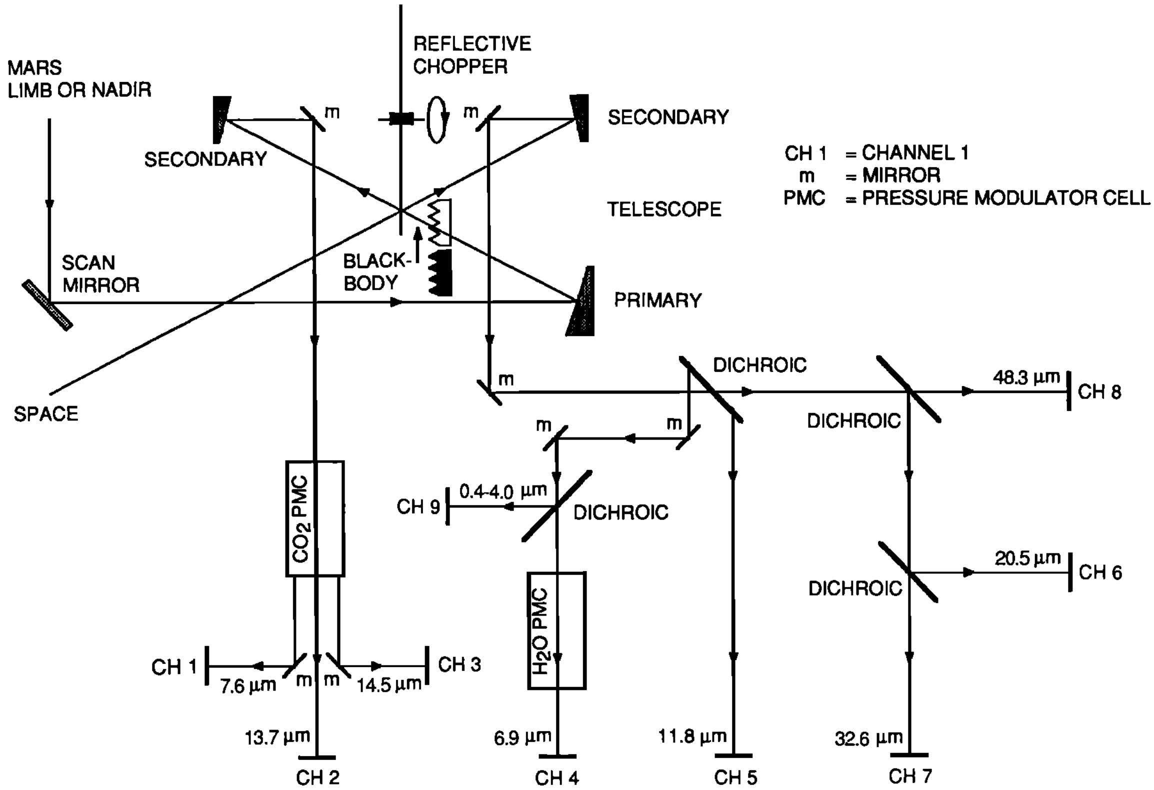

Fig. 4. Pressure modulator infrared radiometer schematic optical layout.

spectral, and FOV characteristics of each channel are determined. PMIRR calibration measurements fall into five basic categories. These are (1) radiometric calibration, (2) linearity calibration, (3) field-of-view calibration, (4) wavelength calibration, and (5) PMC spectral response calibration.

These categories are addressed through both in-flight and laboratory calibration. In-flight calibration is used to correct for small, time-varying changes in the properties of the instrument, whereas laboratory calibration is required to relate in-flight calibration sources to absolute standards and

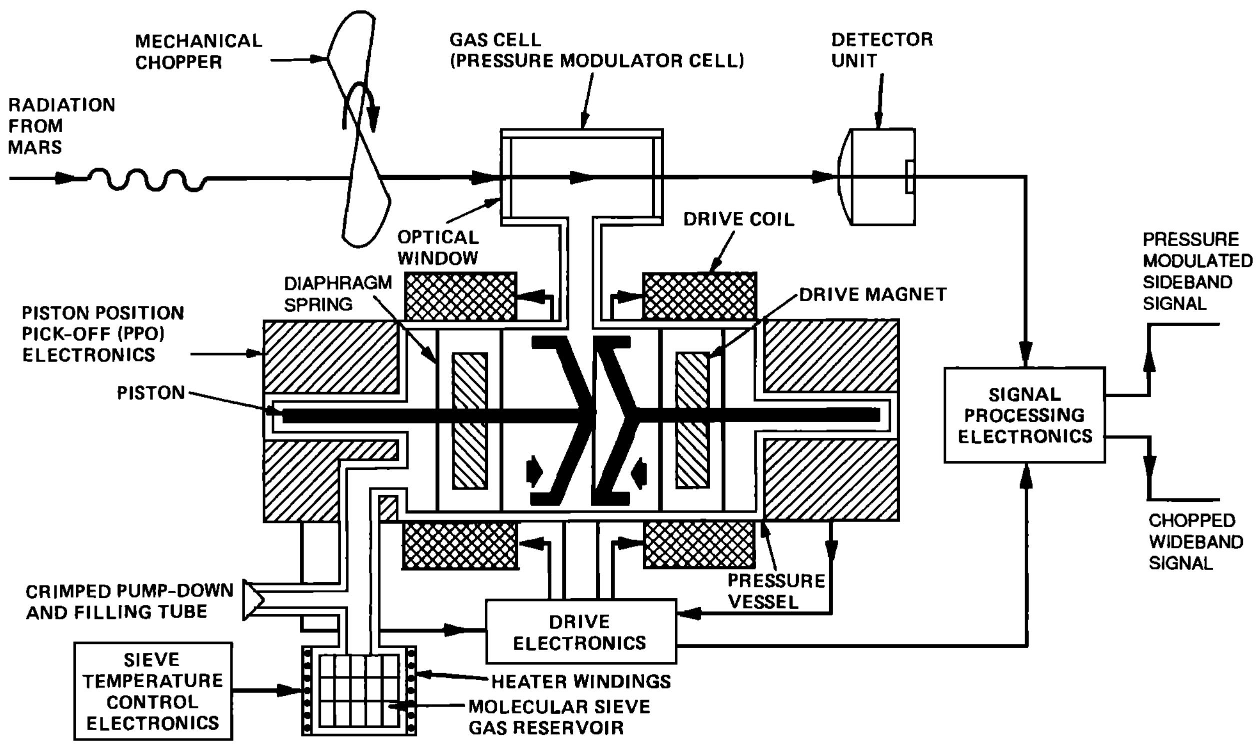

Fig. 5. Schematic of a pressure modulator radiometer channel emphasizing mechanics of the pressure modulator unit.

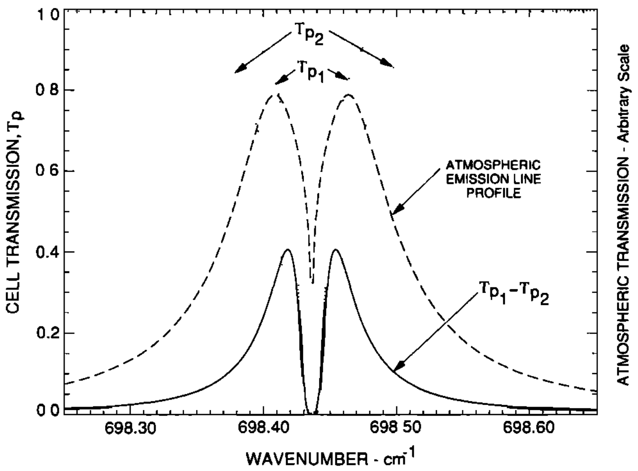

Fig. 6. The spectral discrimination of a pressure modulator radiometer (PMR) for the CO_2 line at 698.436 cm^{-1}. The pressure modulator cell is 3.7 cm long and contains CO_2 at a mean temperature of 300 K modulated between pressures of p_1 = 60 mbar and p_2 = 120 mbar. Atmospheric emission (dashed curve) is calculated for a limb view of the Martian atmosphere at 40 km tangent height, using the Committee on Space Research (COSPAR) standard model temperature profile. Dotted curves show cell transmission profiles at the two pressure extremes. The solid curve is the difference between these profiles and represents the spectral response of the PMR.

to measure instrument calibration parameters that are not expected to change during the mission.

In-flight calibration. Radiometric calibration is the only calibration activity performed during flight, and provisions for accurate radiometric calibration have played a major role in the PMIRR instrument design. The calibration goals for PMIRR are an absolute radiometric accuracy ±0.5% for the thermal infrared channels and ±3% for the solar channel, and a radiometric precision of ±0.1% for all channels.

Absolute calibration is provided for the full dynamic range of each channel by measurements which establish radiometric offset and gain. The offset calibration is supplied by a view of space, which is an excellent radiometric zero for every channel. Gain calibration is achieved using an internal 300 K blackbody for the thermal channels and an external diffusely scattering target for the solar channel. Radiometric precision is obtained by minimizing signal drifts. This is achieved by chopping all signals against space at 800 Hz and by accurately controlling the PMIRR scan mirror and optical bench temperatures.

During flight the PMIRR thermal channels are calibrated at 10-min intervals by views of space and of the internal blackbody, which is a small convoluted cone that is introduced into the optical path of the instrument by an actuator. The accuracy of the gain calibration depends entirely on the accuracy with which emission from the target is known. In order to meet the calibration goals, the effective emissivity of the internal blackbody must exceed 0.995 from 6.5 to 53 μm and its temperature must be monitored to an absolute accuracy of <0.25 K. A high effective emissivity is achieved by treating the surface of the target with a high emissivity coating and by ensuring that the target and the instrument optical cavity that surrounds it are at the same temperature.

The solar channel is calibrated using views of space and the external, diffusely scattering target illuminated by the Sun. The target is an electric arc-sprayed aluminum disc which fills the instrument aperture and FOV. The disc is viewed via the scan mirror once per orbit as the spacecraft approaches the terminator over the northern hemisphere of Mars. The gain calibration depends entirely on the accuracy with which the target reflectivity (absolute) and bidirectional reflectance function can be determined. These were measured in the laboratory, and the target is subsequently protected against contamination by a reclosable cover throughout the launch, cruise, and orbit insertion phases of the mission.

During the mapping orbit, a novel calorimetric method is used to measure any changes in target reflectivity that might occur. The target disc is thermally isolated from the instrument, and its temperature is monitored continuously. Any long-term changes in maximum temperature not consistent with the dominant heat balance terms of solar absorption, thermal emission, and conductance to the instrument are assigned to changes in target reflectivity.

Laboratory calibration. The laboratory radiometric, linearity, FOV, and wavelength calibration of the PMIRR were performed in a thermal vacuum chamber under conditions designed to approximate as closely as possible the instrument environment during a Mars Observer mapping orbit. The sources and targets viewed during calibration were also mounted within the chamber.

TABLE 3. Levels of Data Taken by the Pressure Modulator Infrared Radiometer

Level	Data
0	PMIRR data numbers
1	PMIRR calibrated radiances, calibration files, housekeeping records, and geometry files
2	geophysical fields: surface parameters in the on-planet fields of view and vertical profiles of atmospheric fields associated with individual limb scans
3	globally mapped fields
4	highly derived fields (e.g., diabatic heating and winds)

PMIRR is pressure modulator infrared radiometer.

3.4. *Standard Data Products*

The continuous data taken by PMIRR is processed to five standard levels defined in Table 3. The PMIRR data are organized into packets by the instrument and held by the spacecraft Payload Data System until transmitted to Earth. Level 0 data consist of the PMIRR data packets, together with instrument health parameters stripped from the spacecraft engineering data stream. The level 0 data are checked, assigned a quality flag, and converted into calibrated radiances. These calibrated radiances, calibration files, housekeeping records and associated geometry fields form the level 1 data set. Geometry consists of absolute pointing predictions or knowledge as supplied by the Mars Observer project.

Calibrated radiances are separated into space, limb, partially on-planet, on-planet off-nadir, and on-planet nadir segments. On-planet views associated with the physical space traversed by the limb scans are identified. Atmospheric profiles of temperature, dust extinction, water vapor, haze distribution, and visible reflectance are then retrieved using pressure as a vertical coordinate. These profiles, together with surface fields, form the level 2 data set. The level 3 data set contains individual atmospheric profiles and surface fields which have been combined into global maps, accumulated for various time periods: daily, mapping cycle or monthly, and annual. Two techniques for estimating synoptic maps each day from the asynoptic data acquired from the polar orbiting Mars Observer are currently being investigated: sequential estimation [*Rodgers*, 1976] and asynoptic Fourier transformation [*Salby*, 1982*a*, *b*]. More highly derived products are then computed from these mapped fields (e.g., wind shears, atmospheric heating), and these form the level 4 data set.

3.5. *Observational Approach*

PMIRR measurements are accumulated continuously and repetitively throughout the mapping mission in order to assemble the necessary climatological data set. Functionally, the PMIRR instrument has a single operational mode. Measurements are integrated simultaneously in each channel and are obtained every 2 s, regardless of the position of the scan mirror. This yields a constant data rate of 156 bits per second (bps).

Observational flexibility is provided by the two-axis scan mirror. Because of the repetitive nature of PMIRR's observations the mirror actuators are driven by simple tables in instrument memory. When PMIRR arrives at Mars, it will contain in its memory a nominal set of all tables required to meet its basic measurement objectives. The preloaded tables are read from ROM to RAM, where they can be altered by uplink commands to change the mix or duration of the observational sequence modes. These basic observational modes are reviewed below, following a brief discussion of the limb sounding approach.

Limb sounding. The limiting vertical resolution of a passive remote sounding measurement is determined by viewing geometry, the pressure dependence of atmospheric opacity in the wavelength interval selected, and the instrument signal-to-noise ratio. In practice, the vertical resolution of a limb measurement is determined by the instrument field of view, and current flight systems achieve better than one-half scale height resolution. By contrast, the vertical resolution of a nadir measurement typically approaches an atmospheric scale height. In limb sounding, the effective averaging distance along the line of sight also depends on the instrument field of view and the pressure dependence of atmospheric opacity in the selected wavelength interval. For PMIRR the line-of-sight averaging is approximately 240 km, centered about the tangent point.

Limb sounding enhances sensitivity to (and thereby extends vertical coverage for) atmospheric trace species by increasing the mass-weighted geometrical optical path observed relative to nadir sounding (by a factor of 45 in the case of Mars). Of course, this increased path also enhances the line-of-sight opacity of airborne dust. Although dust opacities are smaller at infrared wavelengths than in the visible, the dust contribution must still be taken into account when processing PMIRR data (see sections 3.2, and 4).

The species sensitivity of a limb sounder is not influenced significantly by the vertical atmospheric temperature gradient. For nadir sounding, in contrast, errors in derived profiles and abundances increase rapidly as the surface and atmosphere become more nearly isothermal. Such conditions are far from rare in either the terrestrial or Martian atmosphere.

Nominal observational sequence. In its primary observation mode, PMIRR looks beneath the spacecraft to view the atmosphere at the aft (in-track) limb, scanning down onto the planet; it then slews further onto the planet to obtain an on-planet, off-nadir view at ≈60° emission angle, followed by a nadir view (Figures 7 and 8). The mirror then slews up to obtain a space view for calibration, and the sequence is repeated. Over the polar regions the repetitive in-track scanning described above is interleaved with "buckshot" sequences which consist of nadir and off-nadir measurements made over a wide range of elevation and azimuth angles using the two-axis scan mirror. This pattern provides nearly optimum coverage of the surface bidirectional reflectance distribution function.

For limb scanners the tangent point recedes as the instrument views lower in the atmosphere. When PMIRR observes the aft limb, this recession of the tangent point is partly compensated by the forward motion of the Mars Observer spacecraft during the 2-s integration time at a given altitude (Figure 8). Thus downward scanning of the aft limb produces a more compact profile in latitude. The effective horizontal resolution achieved when PMIRR views the aft in-track limb is ~4° in latitude, determined by the line-of-sight averaging, and ~28° in longitude at the equator, determined by the 12-13 orbits of Mars Observer each day (Figure 9). Equivalently, longitudinal structures having zonal wavenumbers (i.e., the number of maxima or minima around a latitude circle) ≤6 can be characterized.

A combination of repetitive aft limb scanning and polar "buckshot" sequences constitutes the normal observational mode, whose daily coverage is illustrated in Figure 9. The nominal limb scanning sequence provides contiguous vertical coverage from 90 to −20 km on the limb in 5-km steps (Figure 8). This extended scanning allows each channel to observe the necessary height range while accommodating uncertainties in spacecraft attitude. In the time taken to complete this sequence the spacecraft moves 115 km. Given a line-of-sight averaging of 240 km, it is possible to interleave other observation modes with the in-track limb without seriously compromising latitudinal coverage. Alternatively, successive scans can be averaged together to increase the signal-to-noise ratio when required.

The polar spatial coverage provided by a single day of "buckshot" sequences is shown in Figure 10; this pattern also provides the angular coverage required for polar radiative balance studies. Since the aft limb tangent point is approximately 25° of latitude behind the nadir view location, the aft limb scans become less frequent in middle and high latitudes as the "buckshot" mode is executed at polar latitudes; one should also note that the planetary rotation slightly offsets the on-planet views from the points beneath the aft limb tangent points (Figure 9).

Special-purpose sequences. Buckshot and specialized surface sounding sequences will be employed occasionally at low latitudes to supplement the nadir observations included in the nominal in-track limb and nadir scan. Other special purpose sequences include off-track and cross-track limb scans to give increased local time of day coverage and greater longitudinal or latitudinal resolutions. Figure 11 shows the local times of day accessible by PMIRR. The spacecraft track and thus the trace of PMIRR's nominal observations (with in-track aft limb scanning) are near 0200 and 1400 LT, except near the poles. Local times as much as 1.7 hours earlier and later are accessible by viewing cross track, that is, toward the side limbs orthogonal to the

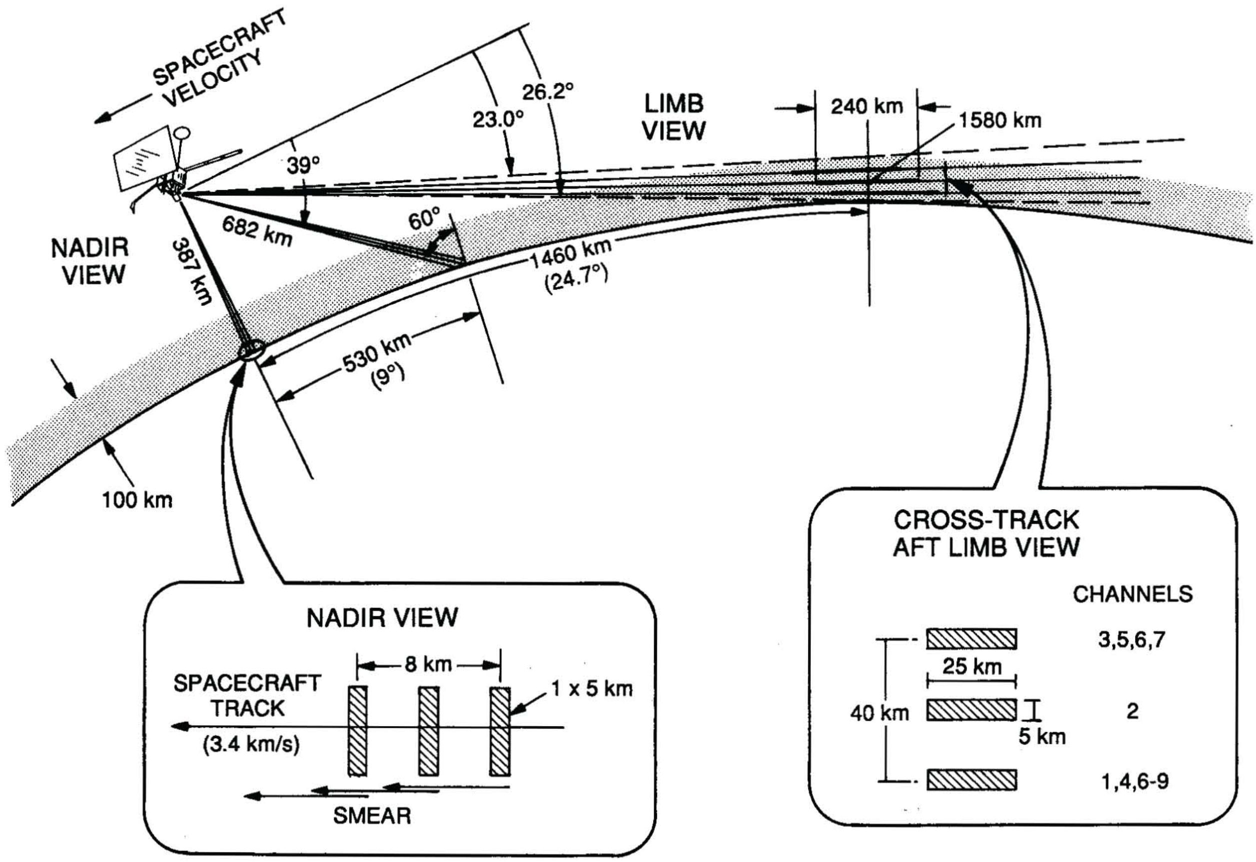

Fig. 7. Observing geometry for the nominal observation mode of the pressure modulator infrared radiometer. The instrument instantaneous field of view (FOV) consists of three detector FOVs projected simultaneously. These are stepped down the aft limb onto the surface and then to on-planet FOVs at local zenith angles of 60° and 0° (nadir). The FOV is then slewed up for a space view, and the sequence is repeated. Insets show the instantaneous footprints at the aft limb and at nadir. Line-of-sight averaging at the limb is ~240 km, or 4° along a great circle.

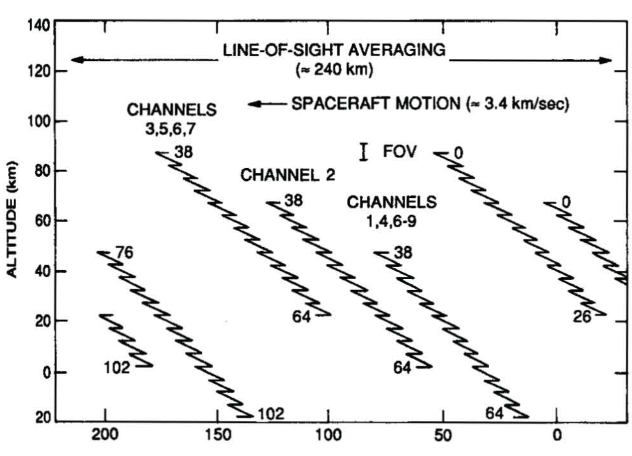

Fig. 8. Locations of the projected centers (tangent points) of the three pressure modulator infrared radiometer detector fields of view (FOVs) when scanning down the aft limb of Mars as part of the nominal observational sequence. Numbers at the beginning and end of each limb segment indicate elapsed time (in seconds) from an arbitrary starting point. Note that the three scan segments are simultaneous, though displaced both vertically and horizontally from one another. The line-of-sight averaging distance when viewing the aft limb is indicated at the top and the height of a single FOV is also shown.

spacecraft track. Above 60° latitude, nearly all local times can be viewed. The FOV rotates slightly when projected onto the side limb, producing lower vertical resolution (~7 km), while achieving much finer latitudinal resolution (~0.5°). In this mode of scanning, line-of-sight averaging (now more zonal) remains 240 km.

The number of steps in the limb scans are programmable, and thus dwell times at a given position which are multiples of the minimum 2 s can be achieved. Each FOV can be stepped by half its vertical dimension (~2.5 km at the aft limb) to explore for finer scale vertical structure. Also, the mix of nadir, on-planet, and limb views can be changed as conditions require. However, the need to obtain a long record with systematic coverage of the meteorological fields means that the special purpose sequences will necessarily be interleaved with the nominal observational sequence.

Coordinated observations. PMIRR will carry at launch specialized sequences for coordinated measurements with other experiments. Coordinated measurement with the radio science (RS) investigation will provide the best means of validating PMIRR's temperature retrieval algorithms. The RS temperatures are particularly valuable as they are derived from measurements of physically independent parameters (i.e., refractive index as opposed to thermal emission) and have very high vertical resolution (~1 km). In the

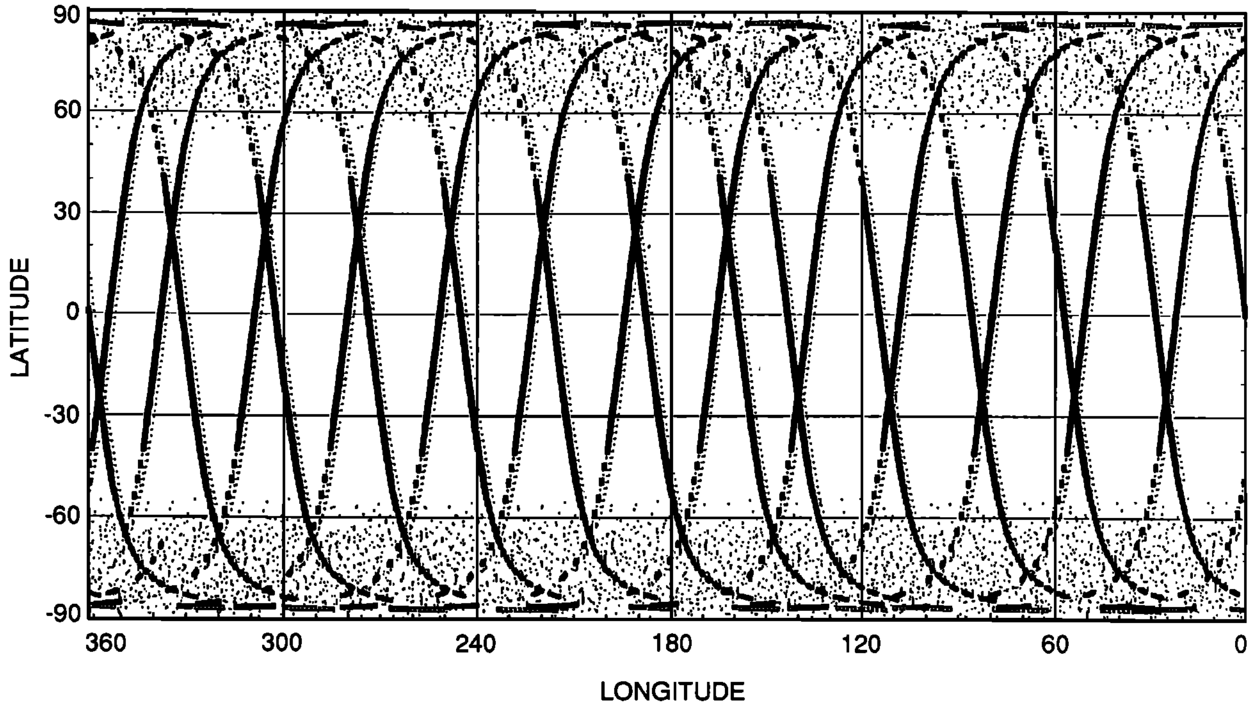

Fig. 9. Daily coverage of Mars achieved during the nominal observational sequence of the pressure modulator infrared radiometer. Each dot represents an on-planet view, while the heavy dashes indicate the horizontal range of tangent points during an aft limb scan. The latter run together at low latitudes but are fewer in number (and so separate) as the spacecraft moves over the polar regions and the "buckshot" mode commences. Nadir views are acquired more than 8 min earlier than the limb scan at the same latitude, and so their longitudes are separated by the rotation of Mars.

southern hemisphere, off-track limb scans allow PMIRR to make nearly simultaneous measurements of the same parcel of atmosphere sampled by radio occultation. Since it cannot view the forward limb, PMIRR views near the occultation tangent point seen by RS in the northern hemisphere some 10–20 min after the occultation has occurred.

TES views the forward in-track limb on a regular though infrequent basis. Thus both PMIRR and TES look at the in-track limb but in opposite directions. PMIRR cross-track limb scanning, interleaved with in-track measurements, will be used to make limb measurements coincident with those obtained by the MOC wide-angle camera. MOC observations of the limb can reveal with 2-km vertical resolution tenuous hazes known to exist from Mariner and Viking limb imaging [*Jaquin et al.*, 1986]. When superimposed on the 5-km resolution PMIRR profiles, these data will yield additional information on the vertical structure and saturation state of the atmosphere.

4. Retrieval Approach and Simulated Results

This section describes how atmospheric profiles and surface properties are retrieved from PMIRR data, given the instrument characteristics and observational strategy discussed above. One means of assessing the anticipated impact of PMIRR data is through retrieval simulations using synthetic radiance data. Such simulations have been carried out for PMIRR, and representative samples are shown here.

4.1. *Retrieval Procedure*

The retrieval of atmospheric variables from remotely sensed infrared radiances requires the solution of a nonlinear

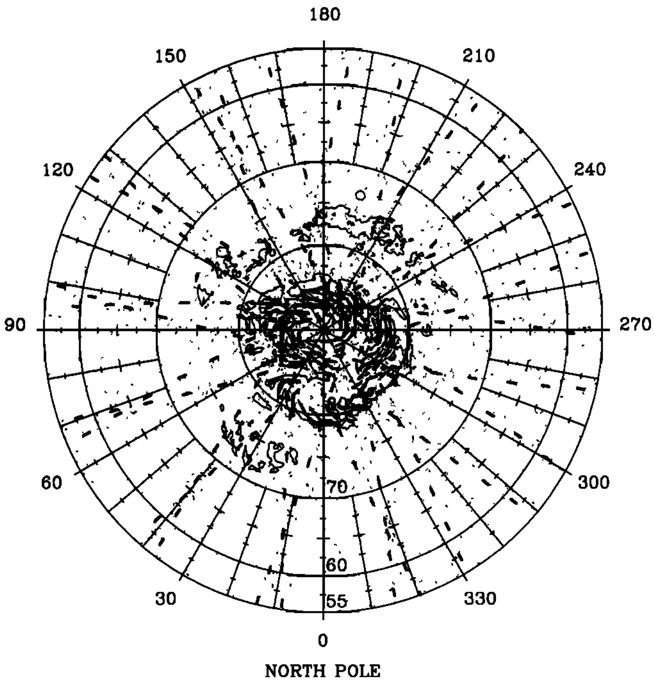

Fig. 10. Daily coverage of the Martian north pole achievable with an extended "buckshot" mode. (The nominal pattern can be seen in Figure 9.) Coverage is shown superimposed on the outlines of the residual ice cap. Each point represents a pressure modulator infrared radiometer on-planet measurement in nine spectral channels. Line segments indicate the horizontal trace of tangent points for limb scans taken as part of the "buckshot" mode. Note the nearly random coverage of the on-planet views.

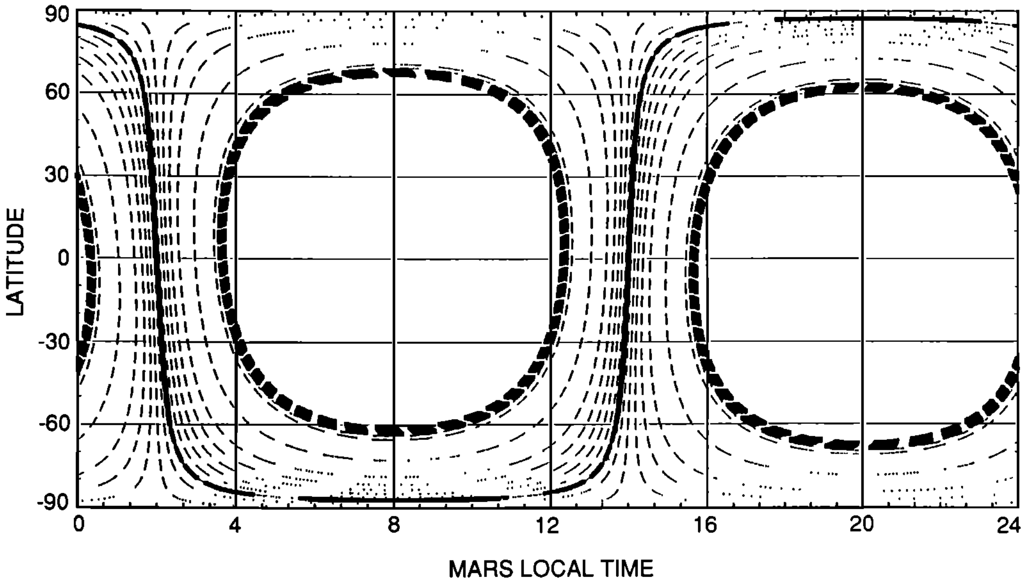

Fig. 11. Local times of day accessible to the pressure modulator infrared radiometer (PMIRR). The positions shown indicate local times that could be viewed during a day in which PMIRR systematically scanned out to both side limbs, as well as to the aft limb. Dots and dashes indicate on-planet measurements. The heavy dashes show local times for the aft limb views and for the side limb tangent points.

radiative transfer equation, namely, a Fredholm integral equation of the first kind. The technique used by PMIRR is the iterative relaxation method [*Chahine*, 1970]. This method starts with initial assumptions for surface temperature and pressure and for the atmospheric profiles of temperature and dust extinction. Instrument radiances are then calculated using these fields as input to a forward radiative transfer model. The assumed profiles are updated using perturbations based on the difference between the calculated and measured radiances.

The profiles input to the forward radiative transfer model are perturbed at levels corresponding to the peaks of the weighting functions, and the updated profiles are constrained by linear interpolation between these levels. This approximation relies on the mean value theorem and works best for narrow, spatially independent weighting functions. At one-half scale height vertical resolution, PMIRR provides a near optimum set of spatially independent samples of the Martian atmosphere, and tests show that within the range covered by these samples, the retrieved profile is insensitive to the initial estimate. After the input fields are perturbed, new instrument radiances are calculated and compared with the observed radiances. This process is repeated iteratively until the measured and calculated radiances converge to within the noise of the measurement.

Iterative retrieval methods of this kind require no climatological information (a distinct advantage for Mars), work well for nonlinear problems, and can be adapted easily to apply ad hoc physical constraints to retrieved profiles. Their chief disadvantages are the greater use of computer time, the lack of formal error statistics associated with the retrieved profile, and their limited ability to make full use of a priori information, when available. Considerable effort is being devoted to making the PMIRR retrieval scheme computationally fast, so that retrievals can keep pace with the rate at which data are received during the mission.

Temperature. Figure 12 shows the vertical response or weighting functions for the three PMIRR temperature sounding channels and a single limb scan. Field-of-view (FOV) averaging has been included. PMIRR sounds temperature using a novel approach in which three pressure modulator radiometer channels observe different spectral emissions features of CO_2 by viewing through a single PMC containing a known mixture of CO_2 isotopes. This cell, 3.7 cm long, has a total pressure of 80 mbar.

In the lower atmosphere, where the amounts of CO_2 along the limb path are extremely large, measurements are made near 7 μm in the weak fundamental ν_1 band of the isotope $^{12}C^{16}O^{18}O$. The concentration of this isotope is enhanced in the PMC to increase the pressure-modulated signal component. Models derived from Mariner 9 observations suggest that 7 μm is also a region of minimum dust extinction in the Martian atmosphere (Figure 13) [*Toon et al.*, 1977]. In the middle atmosphere, where CO_2 amounts in the limb path are smaller, measurements are made using the wing and, at higher altitudes, the R branch of the fundamental ν_2 band of the most abundant isotope. At these levels, dust extinction is usually small.

Pressure. All atmospheric profiles derived from PMIRR measurements are referenced to constant pressure levels, independent of uncertainties in the knowledge of the spacecraft attitude. For a given limb view, atmospheric pressure at the tangent height can be derived from the pressure-modulated and wideband signal components of the PMIRR temperature sounding channels, provided the opacity of the path is dominated by CO_2. The ratio of these signal components is insensitive to atmospheric temperature but is a strong function of pressure at the tangent point of the limb path. Pressure and temperature are therefore retrieved simultaneously with a precision limited only by instrument signal-to-noise performance.

For PMIRR the best results are obtained from the 14.6-μm channel in the 30–50 km region because of good signal-to-noise performance and generally negligible infrared dust

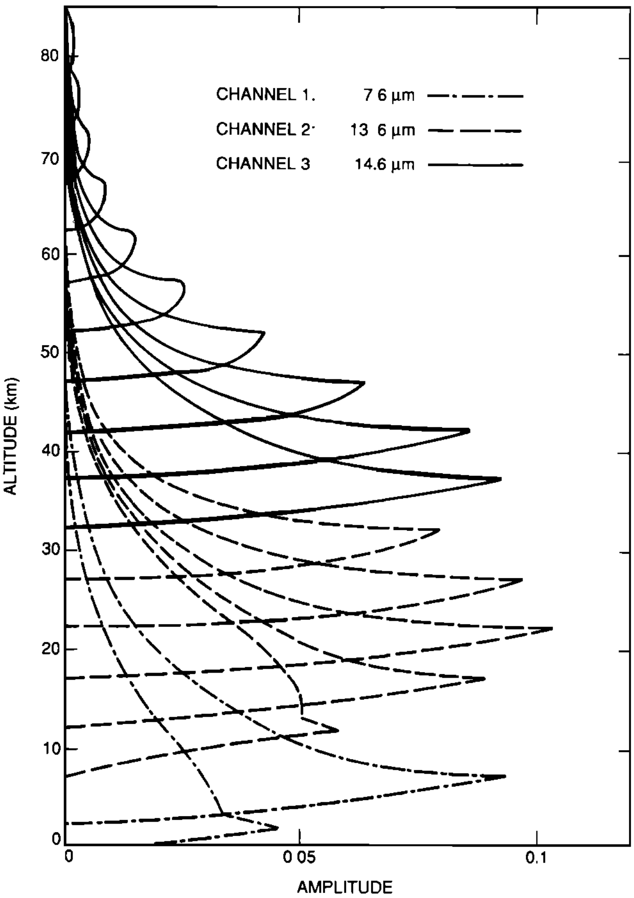

Fig. 12. Pressure modulator infrared radiometer vertical response or weighting functions selected for temperature sounding from limb observations in three spectral intervals. The weighting function is defined by $K(z) = [dT(z, \infty)/dz]$, where $T(z, \infty)$ is the effective transmission from level z to space along the line of sight of the instrument. The response has been calculated for a representative temperature profile at 1-km intervals in height and then convolved with the 5-km vertical field of view of the instrument.

opacity. Given pressures at these altitudes, pressures at other levels are derived from the hydrostatic relation using the retrieved temperature profile and the accurate relative altitude scale provided by the PMIRR limb scan steps. Retrieved temperature, dust, and water vapor profiles are then referenced to simultaneously obtained, colocated pressures.

The pressure retrieval capabilities of PMIRR are similar to those of Earth-orbiting limb sounders such as SAMS on Nimbus 7. This instrument retrieved pressures to approximately 1.5% using temperature-sounding CO_2 pressure modulator channels [*Barnett et al.*, 1985]; PMIRR should do as well as Mars for altitudes above 40 km in the absence of significant dust or condensate haze at those altitudes. Estimation of surface pressure is limited in part by the difficulty of locating the surface at the limb within PMIRR's finite field of view.

PMIRR can retrieve changes in surface pressure with a precision that depends on the contrast between atmospheric and surface temperatures. By combining nadir and limb sounding observations, it is estimated that PMIRR will detect changes in surface pressure with a typical precision of 4%. The absolute accuracy of surface pressure measurements is influenced by uncertainties in surface emissivities and in the spectroscopy of CO_2 over the inhomogeneous nadir path. Systematic errors will be reduced by intercomparison with the thermal emission spectrometer (TES), to better determine surface characteristics, and with the radio science (RS) experiment, which derives temperatures from spacecraft occultation data. PMIRR utilizes its two-axis scanning mirror to observe the atmosphere near the tangent points of the occultation path; for Mars Observer the RS occultations occur at high latitudes.

Non-LTE. Radiative transfer models of the Martian atmosphere indicate that local thermodynamic equilibrium (LTE) in the fundamental ν_2 band of CO_2 will hold to 70 km and perhaps higher. Under non-LTE conditions atmospheric emission is represented not by the Planck function but by a band source function which is determined by a complex balance between radiative, vibrational, and translational excitation and relaxation processes for that band. The effect of non-LTE on PMIRR temperature retrievals is likely to be negligible below 70 km. At greater heights, non-LTE can be taken into account using models of the ν_2 band source function. The day-night contrasts measured by PMIRR at high altitudes should yield information on non-LTE radiative transfer processes in the upper atmosphere of Mars, since solar photons absorbed in the near-IR bands of CO_2 can be

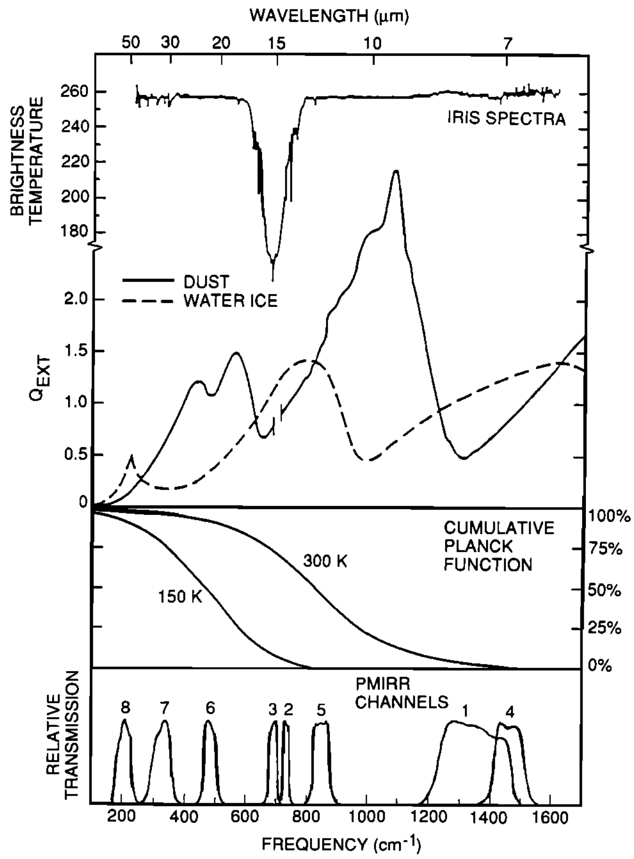

Fig. 13. Pressure modulator infrared radiometer spectral channel locations compared with cumulative Planck functions and with the wavelength variation of atmospheric extinction due to suspended dust or to water ice, as computed for representative particle size distributions and compositions [*Toon et al.*, 1977; *Curran et al.*, 1973]. Absorption by CO_2 gas is indicated by the Mariner 9 IRIS spectrum [*Hanel et al.*, 1972].

exchanged as vibrational quanta which are reemitted in the 15-μm band.

Dust and condensate extinction profiling. PMIRR measures aerosol extinction profiles in eight spectral channels covering the range 6.5–50 μm. These profiles are derived from dust channels measuring limb emission measurements simultaneously and with the same vertical and horizontal resolution as the temperature-sounding channels. Observations from the Mariner 9 and Viking spacecraft have shown that the infrared opacity of airborne dust is strongly dependent on wavelength [*Toon et al.*, 1977; *Martin et al.*, 1979] and have allowed opacities at infrared and visible wavelengths to be related [*Zurek*, 1982; *Martin*, 1986]. Models derived from this data have been used to guide the spectral placement of PMIRR channels and to relate opacities in different channels. For altitudes with relatively low dust opacity, estimates of the dust optical depth can be made independent of a priori knowledge of dust spectral characteristics in those channels having both a pressure-modulated and a wideband signal.

Four PMIRR spectral channels are designed primarily for dust and condensate profiling (Figure 13 and Table 1). Channels at 11.8 and 20.5 μm are chosen for their contrasting sensitivity to small amounts of water ice and dust. The channel at 32.6 μm, located in a spectral interval where gaseous absorption is negligible, serves as a reference for total line-of-sight opacity due to airborne particulates. Two detectors in the 20.5-μm channel and two detectors in the 32.6-μm channel cover the full height range (Figures 7 and 8 and Table 1). Water ice hazes are observed throughout this range by the combination of the 11.8- and 48.3-μm channels. The latter is particularly useful when dust opacities are high. The 32.6- and 48.3-μm channels have contrasting sensitivities to water vapor, water ice, and dust, but both are less sensitive to dust and condensates having the size distributions and number densities expected in the Martian atmosphere than are the 11.8 and 20.5 μm channels. Figure 13 compares the spectral location of all the PMIRR infrared channels with extinction spectra for dust and water ice, computed using particle sizes suggested by Mariner 9 and Viking orbiter observations [*Toon et al.*, 1977; *Curran et al.*, 1973].

The independent retrieval of temperature in the presence of particulates is essential for reliable dust and condensate profiling and is made possible by the two signal components of the pressure modulator temperature-sounding channels. Because the pressure-modulated and wideband signal components share fields of view and spectral band passes, they have identical responses to emission from particulates. The large contrast in response to CO_2 emission for the two signal components therefore allows particulate and CO_2 emission to be differentiated by each temperature sounding channel, once pressure is determined in that field of view.

Given the vertical profile of temperature as a function of pressure, profiles of the extinction due to dust and condensates are derived from limb and nadir emission measurements made in each PMIRR infrared channel. Both thermal emission and scattering contribute to particulate radiance. As particle single-scattering albedos are small at infrared wavelengths, the primary scattering of upwelling radiation from the surface dominates the scattering source function. Multiple scattering is unlikely to be significant. Under these conditions multispectral extinction profiles can be retrieved and used to distinguish between dust and condensates and to investigate their microphysical properties.

PMIRR will also measure on-planet and limb radiances in its broadband solar channel (Table 1). When it views the limb, the solar channel will observe solar radiation scattered to the instrument by atmospheric hazes, and the measured radiances can be used to locate the altitudes of the hazes and to constrain their visible opacities [e.g., *Jaquin et al.*, 1986]. A direct measurement of the visible broadband solar extinction can be made over the north polar region on those occasions when PMIRR views its solar calibration target as Mars Observer approaches the terminator from the night side. At those times the solar calibration target, which faces the forward limb, is illuminated by the rising Sun occulted by the Martian atmosphere. Finally, combining on-planet views of the broadband solar channel which have different reflection and incidence angles provides some constraints on the broadband visible opacities and scattering properties of suspended dust and the reflectance of the surface itself [e.g., *Thorpe*, 1977]. On-planet views of the solar channel also allow PMIRR to monitor the advance and retreat of the seasonal polar caps [e.g., *Christensen and Zurek*, 1984] and, through surface albedo changes, the redistribution of surface aeolian materials [e.g., *Christensen*, 1988].

Water vapor profiling. PMIRR derives water vapor profiles from emission measurements in channels centered at 6.9 and 48.3 μm in the spectral features of H_2O. These measurements are coincident with and have the same spatial resolution as those of temperature and particulates.

The 6.9-μm channel is centered in the near wing of the H_2O ν_2 vibration-rotation band, close to a minimum in the dust opacity spectrum, and uses pressure modulation radiometry to achieve high sensitivity to water. The pressure modulator cell is 10 cm long and contains H_2O at a pressure of 17 mbar. Water vapor concentration and 6.9-μm dust extinction are retrieved independently from the pressure-modulated and wideband components of the 6.9-μm signal, given the temperature profile retrieved using other channels. The 48.3-μm channel is located in the water vapor rotation band and employs simple passband filter radiometry. At this wavelength the channel is relatively insensitive to dust opacity and has less sensitivity to a given temperature error, as determined by the Planck function. Thus the 48.3-μm channel can be used to augment water vapor profile retrievals derived from measurements with the 6.9-μm channel. For low water abundances ($\leq$10 pr μm) and background dust opacities the 6.9-μm channel yields the best results, whereas the 48.3-μm channel is better suited to dustier conditions and greater water abundances.

Polar radiative balance. The PMIRR solar and infrared channels measure directly the solar and infrared radiation emerging from the top of the Martian atmosphere. The spectral response of the PMIRR solar channel covers 97% of the incident solar flux. Observations in this channel, obtained over a wide range of viewing geometries via the articulated scan mirror, will be used to determine the bidirectional reflectance of the surface-atmosphere system. Multispectral measurements in the eight PMIRR infrared channels will be used to synthesize bolometric emission spectra as a function of emission angle.

Figure 13 shows the spectral location of the PMIRR infrared channels relative to the cumulative Planck functions for 150 and 300 K blackbodies. Errors in net emission produced by the necessary interpolation and extrapolation of emission spectra are expected to be small because the bolometric integral is well sampled by PMIRR. Errors in modeling the surface heat balance are reduced given observations of the upward flux at the top of the atmosphere at several different wavelengths and using atmospheric properties derived from simultaneous PMIRR observations. Studies using Viking observations have shown that the net flux of solar and IR radiation at the top of the atmosphere dominates the heat balance of the polar atmosphere-surface system during most seasons [*Paige and Ingersoll*, 1985]; this makes it possible to determine condensation and sublimation rates of CO_2 on the surface and in the atmosphere from remote observations.

Surface temperatures. PMIRR will measure on-planet radiances at eight infrared wavelengths as part of its nominal observational mode (section 3.5). When viewing the nadir, a smeared FOV is ~7 km along track and 5 km cross track (Figure 7); channels 6 and 7 (at 20.5 and 32.6 μm) have two FOVs each, and all other surface sensing channels are superimposed on one of these two. In channels 7 and 8 (at 32.6 and 48.3 μm) the radiances are dominated by thermal emission from the surface and also do not exhibit the nonlinear response to nonisothermal surface fields of view, this complicates the interpretation of data obtained at shorter wavelengths. An integral part of the PMIRR data reduction plan is to use these radiances to retrieve the temperature and spectral emissivity of the surface. Surface temperatures can be used to map at relatively coarse resolution (e.g., 2° × 2°) the bulk thermal properties of the Martian surface and to locate surface frost and ice deposits. CO_2 frost deposits can be identified by temperatures close to the CO_2 solid-vapor equilibrium temperature of ~148 K at 6 mbar CO_2 partial pressure.

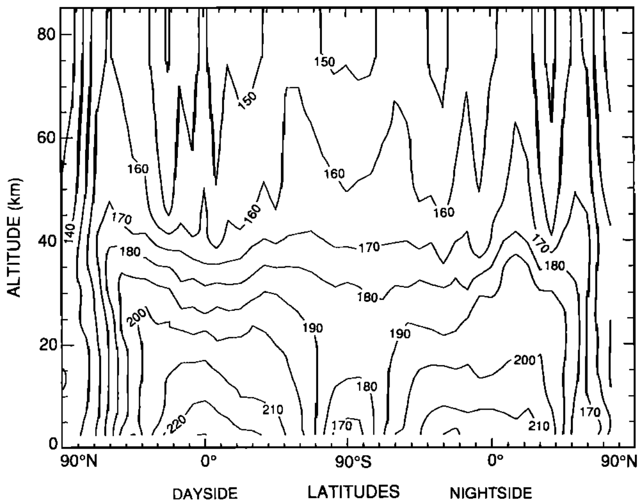

Fig. 14. Temperatures (in degrees Kelvin) used to simulate one orbit of pressure modulator infrared radiometer radiances. Values were taken from a general circulation model (GCM) history tape generated by the NASA Ames Research Center Mars GCM [*Pollack et al.*, 1990] in a simulation of a global dust storm at southern summer solstice; above 40 km these values were merged with temperatures from the Mars Global Reference Atmospheric Model (MARS GRAM) engineering model [*Justus*, 1991] for the same season. Note the cold north polar atmosphere and strong temperature gradients at high latitudes.

4.2. *Anticipated Results*

The ability to retrieve atmospheric profiles from PMIRR radiance measurements cannot be simulated using existing data alone, since those data lack global coverage or adequate vertical resolution and coverage. There are, for instance, very few meridional cross sections of temperature, such as the ones retrieved from Mariner 9 (Figure 1). Furthermore, the region 40–80 km in altitude is virtually unexplored, and typically only column values of dust extinction and water vapor amounts are available (e.g., Figure 2).

For these reasons, retrieval simulations have been extended using atmospheric fields computed by models representing the range of atmospheric conditions anticipated at Mars. From these fields, both observed and computed, synthetic PMIRR radiances are generated to simulate limb and on-planet observations. These synthetic radiances include the appropriate geometrical factors and known instrumental noise. By using the retrieval algorithms now under development, vertical profiles are retrieved from these synthetic radiances and compared with the original input fields.

Temperature, dust extinction, and pressure measurements. Figure 14 shows a synthetic climatology used to assess our ability to retrieve from PMIRR measurements vertical profiles of temperature and dust as a function of pressure. The one-orbit cross section was constructed using vertical profiles of temperature taken from a history tape generated as part of a southern summer solstice simulation by the Ames Research Center Mars General Circulation Model (GCM) [*Pollack et al.*, 1990]. The Mars GCM currently has a longitude-latitude resolution of 9° × 7.5° and extends to ~50 km in altitude. Dayside profiles were taken from the longitude whose local time was closest to 1400 LT, and nightside profiles were appended from the longitude whose local time was closest to 0200 LT. The resulting cross section (Figure 14) thus extends from 90°N through the south pole (dayside, descending portion of the orbit) and back to 90°N (nightside, ascending portion of the orbit). Above 40 km the Mars GCM temperature profiles were smoothly merged with profiles obtained from the Mars Global Reference Atmospheric Model (MARS-GRAM) engineering model [*Justus*, 1991]. Note that PMIRR obtains the coverage shown in Figure 14 for each of 12-13 orbits daily and with a latitudinal resolution of ~4°.

Figures 15 and 16 show the differences between the retrieved temperatures and dust extinction values and the original values input from the model fields, as a function of latitude and height. The dust opacity in the Mars GCM run was specified to have a visible optical depth $\tau_v = 2$, and the dust was assumed to be uniformly mixed with height. In order to examine the effects of different dust concentrations on the combined retrieval of temperature and dust extinction, the synthetic radiances were generated assuming that τ_v varied from 0.5 at the poles to 2 at the equator. This spans a range representative of the background dust loading above the Viking lander sites to that characteristic of a planetary-scale dust storm [*Pollack et al.*, 1979]. As a further challenge to the retrieval algorithm, the vertical distribution of suspended dust was randomly perturbed with height; these variations are evident in Figure 17, where several individual profiles from the simulation run are shown.

Below 80 km, temperature errors in the retrieved profiles are typically 2 K or less (Figure 15), and the percent error in retrieved dust extinction (opacity) is typically 10% or less (Figure 16). The largest errors occurred when the opacity was greatest in the region of transition between channels 1 and 2 (Figure 12). (The large relative errors in Figure 16 above 50 km in the polar regions are due to the very cold, nearly isothermal atmosphere and to the very small amounts of dust assumed to be present at those altitudes.) Errors in retrieved pressures (not shown) are typically 1–2% from profile to profile at those altitudes where dust opacity is not significant. Errors in estimated surface pressure are less than 3% but do not include surface uncertainties and systematic errors in the spectroscopy.

While Figures 15 and 16 are representative of the relative error characteristics of retrieved profiles, not all systematic errors have been included. Additional systematic errors in temperature and pressure retrievals are expected due to uncertainties in the calculation of CO_2 transmittances in the Martian atmosphere. Also, it has been assumed in the simulations that the limb FOVs did not intersect the ground. Sources of systematic errors not accounted for in the simulated dust retrievals include the scattering of surface emission into the limb field of view and the assumed ratio of dust opacity between the various IR wideband (WB) channels. These ratios are needed when the dust loading is so large that the ratio of pressure-modulated to wideband signals essentially saturates and cannot provide an independent estimate of the dust opacity; the variation of dust opacity with wavelength (Figure 13) was computed for the particle size distribution and compositions suggested by the analysis of Mariner 9 and Viking data [*Toon et al.*, 1977; *Hunt*, 1979; *Zurek*, 1982; *Kahn et al.*, 1992].

Water vapor and condensates. Atmospheric condensates have been identified in Mariner 9 and Viking Orbiter visible images of Mars [*Anderson and Leovy*, 1978; *Jaquin et al.*, 1986]. They are thought to be composed of CO_2 and water ices, occur in distinct layers as well as broadly distributed hazes, and may frequently be mixed with airborne dust. PMIRR must therefore identify the different types of Martian aerosols and map their distributions. Figure 18 shows a simulated retrieval of water ice and dust mass loading profiles for dust and ice mixed in the same atmospheric columns. For this test case, dust and condensate mass loadings are determined with a precision of ~20% by extinction measurements in PMIRR channels 5–8. The broadband solar channel can also be used to estimate the optical properties and so constrain the microphysical characteristics of condensate hazes, but this has not yet been included in the operational retrieval algorithm.

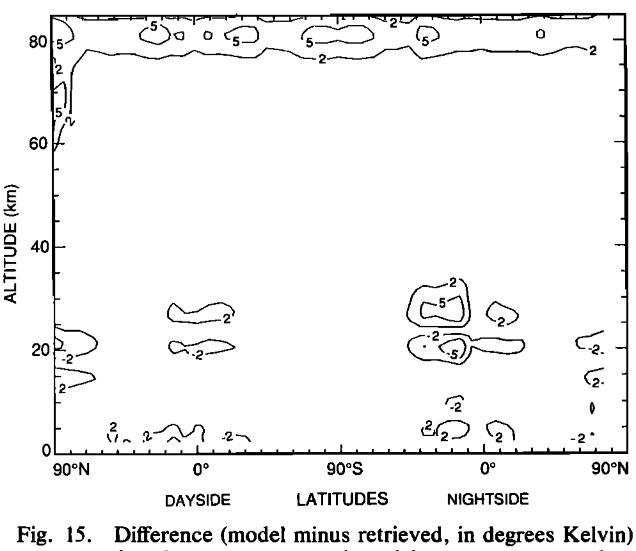

Fig. 15. Difference (model minus retrieved, in degrees Kelvin) between retrieved temperatures and model temperatures used to synthesize pressure modulator infrared radiometer radiances.

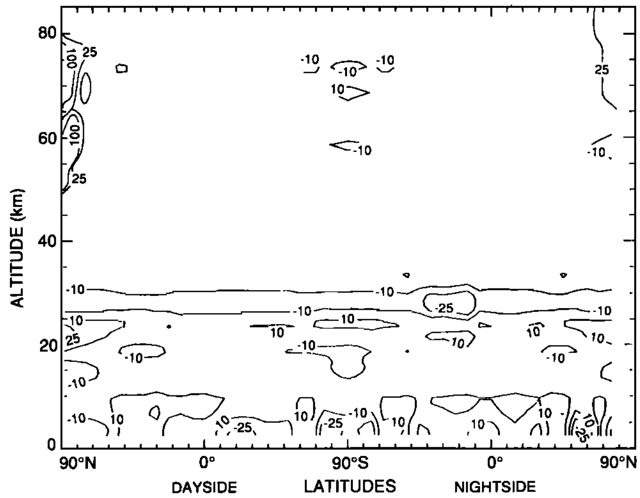

Fig. 16. Relative difference in percent of dust extinction; that is, 100 × [ln (retrieved) − ln (model)]. The assumed column dust amount varies (as a cosine function in latitude) from a channel 1 opacity of $\tau_{7.6\mu m}$ = 0.05 at the poles to a maximum of $\tau_{7.6\mu m}$ = 0.2 at the equator. Visible opacities τ_v (at ~ 0.6 μm) are estimated to be 10 times larger [*Zurek*, 1982]; that is, $\tau_v = 0.5 - 2$.

Given the retrieved temperature profile, water vapor profiles are derived from limb radiance measurements in channels 4 and 8. Figure 19 shows simulated water vapor profile retrievals for two very different temperature profiles. A background column dust visible optical depth of 0.4 is assumed, and the water model is based on the altitude dependence of the saturated vapor pressure of water. Water vapor mixing ratios are retrieved with a precision of 10–20% in the lower atmosphere. The upper limit of PMIRR vertical coverage is determined largely by the atmospheric holding capacity (i.e., saturation vapor pressure for water), which decreases rapidly with decreasing temperature.

Polar heat balance. PMIRR will acquire the spatial, temporal, and angular coverage necessary to determine the reflected and emitted radiation fields in the polar regions by scanning a preselected set of 31 azimuth and elevation angles. Figure 10 shows the spatial coverage that can be obtained over the north pole by PMIRR in just 13 orbits during 1 day. PMIRR observations span most of the range of emission and solar azimuth angles needed to construct the bidirectional reflectance. The main gap in angular coverage is due to PMIRR's inability to see the forward limb. However, this relatively small but important gap is well sampled by TES, which observes in track toward the forward limb with its own solar channel.

CO_2 clouds. Atmospheric temperature profiles provide the most important clue to the existence of CO_2 clouds because, whatever their scattering and emission properties, the temperatures at the tops of these clouds must be at or below the local CO_2 saturation temperature. The pressure levels of the effective top of the clouds can be determined

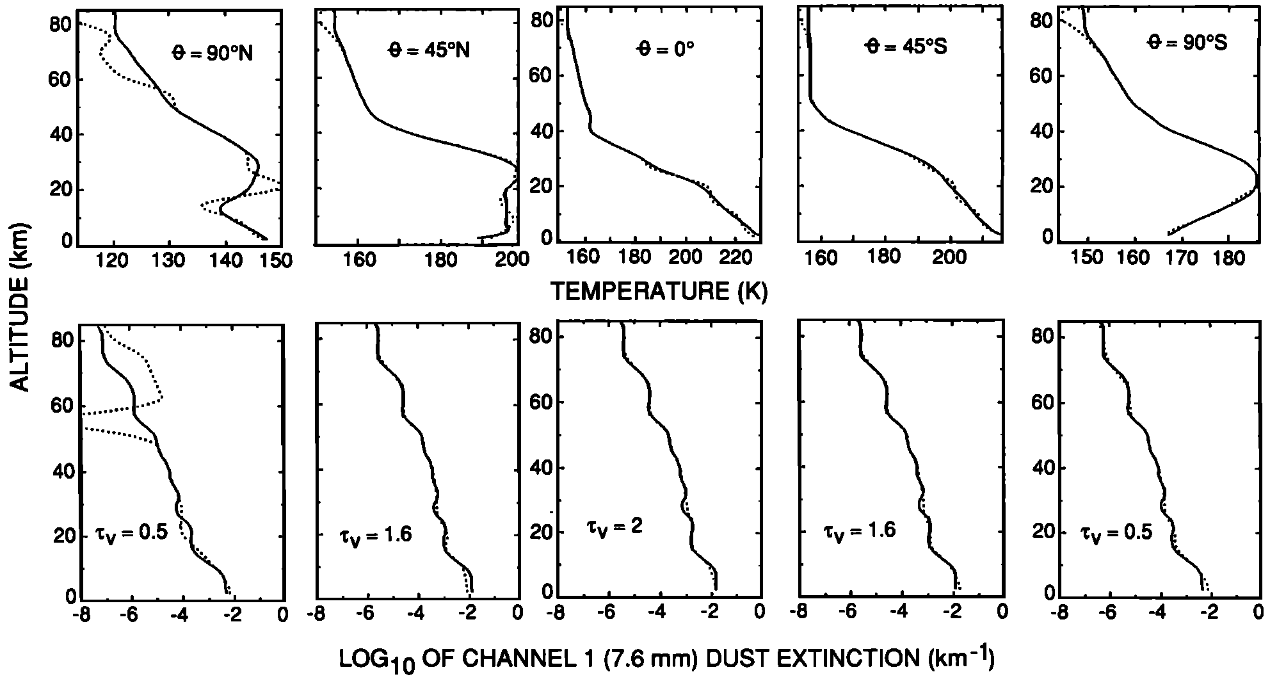

Fig. 17. Individual profiles comparing retrieved (dotted curves) versus model atmosphere (solid curves). Largest errors are encountered above the winter pole because of the low values of thermal emission from the cold polar atmosphere.

using the PMIRR wideband and PMC radiances in channels 1–3. Below the tops of the clouds the PMIRR limb radiances will depend in detail on the optical properties and opacity of the cloud particles. PMIRR's ability to observe at nadir, off-nadir, and limb geometries should resolve whether the anomalously low brightness temperature regions observed by Viking [*Kieffer*, 1979] are due to surface or atmospheric phenomena [*Paige*, 1985]. Vertical profiles of temperature and aerosol extinction would provide useful constraints on the condensation of volatiles in the winter polar atmosphere and the incorporation of dust and water into the seasonal polar caps.

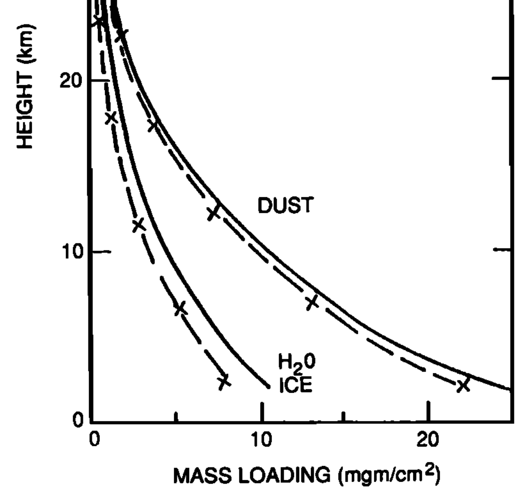

Fig. 18. Simulating the simultaneous retrieval of water ice and dust mass loading.

Surface science. All standard PMIRR observational sequences include regular observations of solar reflectance and infrared emission. Retrieving surface temperatures from these observations will be an integral part of the PMIRR data reduction scheme. During a mapping cycle, the surface coverage obtained by PMIRR will be sufficient to map globally surface temperatures at 0200 and 1400 LT and top-of-the-atmosphere solar reflectances to spatial resolutions of 2° × 2°. At high latitudes, increased temporal and spatial sampling results from the spacecraft orbit and PMIRR's frequent on-planet viewing for polar radiative balance measurements. This will enable PMIRR to obtain maps of surface temperatures and top-of-the-atmosphere solar reflectances to spatial scales of 0.5° × 0.5° every 5 days at high latitudes.

Thermal and reflectance maps derived from PMIRR data can be used to determine (1) the apparent thermal inertia of the surface of Mars from diurnal surface temperature variations [*Palluconi and Kieffer*, 1981], (2) the extent of the seasonal polar caps, (3) the actual surface albedo and surface thermal inertia using one-dimensional radiative-convective models in conjunction with PMIRR-derived atmospheric temperature and opacity fields [*Paige*, 1985], and (4) high-latitude subsurface temperatures and thermal properties using the observed seasonal cycles of surface temperatures.

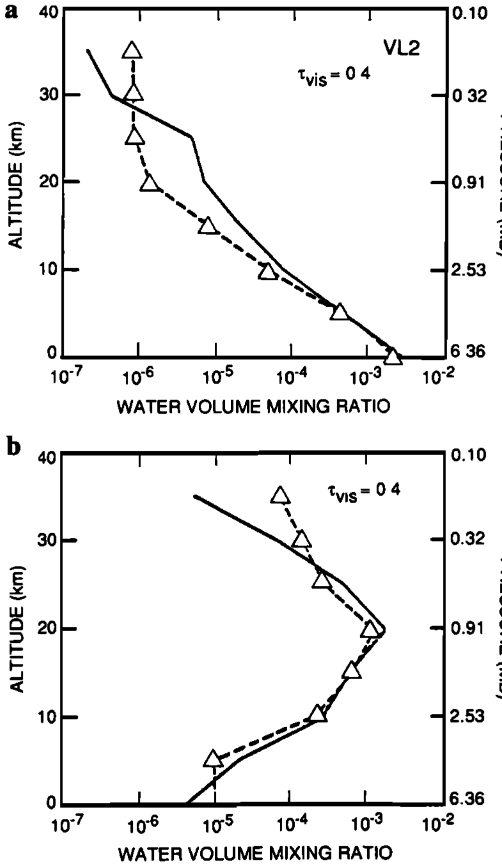

Fig. 19. Simulated retrieval (dashed lines) of water vapor profiles corresponding to (*a*) the Viking lander 2 entry temperature profile [*Seiff and Kirk*, 1977], and (*b*) a radio occultation temperature profile [*Lindal et al.*, 1979]. The vertical distributions of "atmospheric" vapor mixing ratio (solid lines) were constructed using partial pressures needed to give a constant relative humidity.

5. Summary

The exploration of Mars will enter a new phase with Mars Observer. The low, circular, and nearly polar orbit of the spacecraft will provide an ideal platform for the systematic remote investigation of the atmosphere of Mars and its seasonal variation. PMIRR is designed to take full advantage of that platform to map the global fields of temperature, dust distribution, water vapor, surface ice and atmospheric condensates, and the reflected solar and emitted thermal emission at the top of the atmosphere. From these fields we can derive the vertical variation of horizontal winds, the diabatic forcing of the atmosphere, zonal mean transport (i.e., residual mean) velocities, surface radiation components, and key parameters of the surface energy budget, such as the change of CO_2, the surface albedo and the apparent thermal inertia.

The climatologies generated for Mars by PMIRR will be unprecedented in their comprehensive coverage and in their vertical and horizontal resolutions. Just as for the case of Earth, such climatologies provide a basis for seeking an improved understanding of the physical processes underlying the present structure and future change of the atmosphere and climate of Mars [*Zurek and McCleese*, 1989]. We may gain insight into the past climates of Mars and perhaps, through comparative study, of Earth as well. Each of the past spacecraft investigations of Mars has yielded new, and often dramatically changed, perspectives of that planet. Mars Observer is unlikely to be an exception.

Acknowledgments. We gratefully acknowledge the contributions of the following to preparation of this manuscript: S. Calcutt and T. Kingsmill-Vellicott of Oxford University; A. Ono of UCLA; E. Fetzer, S. Gaiser, D. Rider, H. Stone, and R. West of JPL/Caltech. A heartfelt thanks is extended to W. Harris, J. R. Locke, and all those members of the PMIRR hardware team whose contributions to design and fabrication of the instrument make this investigation possible. We also thank J. Pollack, R. Haberle, and J. Schaeffer of NASA Ames Research Center for providing the Mars GCM history tape, as well as L. Chen and J. Knighton of JPL for assisting in the creation of the combined atmospheric model for testing the retrieval schemes. This work was funded by the Mars Observer Project and was carried out at the Jet Propulsion Laboratory, California Institute of Technology, under contract with the National Aeronautics and Space Administration.

References

Anderson, E., and C. B. Leovy, Mariner 9 television limb observations of dust and of ice hazes on Mars, *J. Atmos. Sci.*, *35*, 723–734, 1978.

Andrews, D. G., J. R. Holton, and C. B. Leovy, *Middle Atmosphere Dynamics*, 490 pp., Academic, San Diego, Calif., 1987.

Arvidson, R. E., E. A. Guiness, H. J. Moore, J. E. Tillman, and S. D. Wall, Three Mars years: Viking Lander 1 imaging observations, *Science*, *222*, 463–468, 1983.

Barker, E. S., R. A. Schorn, A. Woszcsyk, R. B. Tull, and S. J. Little, Mars: Detection of atmospheric water vapor during the southern hemisphere spring and summer season, *Science*, *170*, 1308–1310, 1970.

Barnes, J. R., Time spectral analysis of midlatitude disturbances in the Martian atmosphere, *J. Atmos. Sci.*, *37*, 2002–2015, 1980.

Barnes, J. R., Midlatitude disturbances in the Martian atmosphere: A second Mars year, *J. Atmos. Sci.*, *38*, 225–234, 1981.

Barnes, J. R., Finite-amplitude behavior of a single baroclinic wave with multiple vertical modes: Effects of thermal damping, *J. Atmos. Sci.*, *43*, 58–71, 1986.

Barnes, J. R., Transport of dust to high northern latitudes in a Martian polar warming, *J. Geophys. Res.*, *95*, 1381–1400, 1990*a*.

Barnes, J. R., Possible effects of breaking gravity waves on the circulation of the middle atmosphere of Mars, *J. Geophys. Res.*, *95*, 1401–1422, 1990*b*.

Barnes, J. R., and J. L. Hollingsworth, Dynamical modeling of a planetary wave mechanism for a Martian polar warming, *Icarus*, *71*, 313–334, 1987.

Barnett, J. J., et al., Global and seasonal variability of the temperature and composition of the middle atmosphere, *Nature*, *313*, 439–443, 1985.

Briggs, G. A., and C. B. Leovy, Mariner 9 observations of the Mars north polar hood, *Bull. Am. Meteorol. Soc.*, *55*, 278–296, 1974.

Chahine, M. T., Inverse problems in radiative transfer: Determination of atmospheric parameters, *J. Atmos. Sci.*, *27*, 960–967, 1970.

Christensen, P. R., Regional dust deposits on Mars: Physical properties, age, and history, *J. Geophys. Res.*, *91*, 7611–7624, 1986.

Christensen, P. R., Global albedo variations on Mars: Implications for active aeolian transport, deposition, and erosion, *J. Geophys. Res.*, *93*, 7611–7624, 1988.

Christensen, P. R., and R. W. Zurek, Martian north polar hazes and surface ice: Results from the Viking Survey/Completion Mission, *J. Geophys. Res.*, *89*, 4587–4596, 1984.

Conrath, B. J., Thermal structure of the Martian atmosphere during the dissipation of the dust storm of 1971, *Icarus*, *24*, 36–46, 1975.

Conrath, B. J., Influence of planetary-scale topography on the diurnal thermal tide during the 1971 Martian dust storm, *J. Atmos. Sci.*, *33*, 2430–2439, 1976.

Conrath, B. J., Planetary-scale wave structure in the Martian atmosphere, *Icarus*, *48*, 246–255, 1981.

Conrath, B. J., R. Curran, R. Hanel, V. Kunde, W. Maguire, J. Pearl, J. Pirraglia, J. Welker, and T. Burke, Atmospheric and surface properties of Mars obtained by infrared spectroscopy on Mariner 9, *J. Geophys. Res.*, *78*, 4267–4278, 1973.

Curran, R. J., B. J. Conrath, R. A. Hanel, V. G. Kunde, and J. C. Pearl, Mars: Mariner 9 spectroscopic evidence for H_2O ice clouds, *Science, 182*, 381–383, 1973.

Davies, D. W., Effects of dust on the heating of Mars' surface and atmosphere, *J. Geophys. Res., 84*, 8289–8293, 1979.

Davies, D. W., The Mars water cycle, *Icarus, 45*, 398–414, 1981.

Deming, D., M. J. Mumma, F. Espenak, T. Kostiuk, and D. Zipoy, Polar warming in the middle atmosphere of Mars, *Icarus, 66*, 366–368, 1986.

Fanale, F. P., Martian volatiles: Their degassing history and geochemical fate, *Icarus, 28*, 179–202, 1976.

Fanale, F. P., and W. A. Cannon, Mars: CO_2 adsorption and capillary condensation on clays—Significance for volatile storage and atmospheric history, *J. Geophys. Res., 84*, 8404–8414, 1979.

Farmer, C. B., and P. E. Doms, Global seasonal variation of water vapor on Mars and the implications for permafrost, *J. Geophys. Res., 84*, 2881–2888, 1979.

Farmer, C. B., D. W. Davies, A. L. Holland, D. D. LaPorte, and P. E. Doms, Mars: Water vapor observations from the Viking orbiters, *J. Geophys. Res., 82*, 4225–4248, 1977.

Garcia, R. R., and S. Solomon, A numerical model of zonally averaged dynamical and chemical structure of the middle atmosphere, *J. Geophys. Res., 88*, 1379–1400, 1983.

Gierasch, P. J., Martian dust storms, *Rev. Geophys. Space Phys., 12*, 730–734, 1974.

Gierasch, P. J., and R. M. Goody, The effect of dust on the temperature of the Martian atmosphere, *J. Atmos. Sci., 29*, 400–402, 1972.

Gifford, F. A., A study of Martian yellow clouds that display movement, *Mon. Weather Rev., 92*, 435–440, 1964.

Gille, J. C., and J. M. Russell III, The Limb Infrared Monitor of the Stratosphere: Experiment description, performance, and results, *J. Geophys. Res., 89*, 5125–5140, 1984.

Gille, J. C., L. V. Lyjak, and A. Smith, The global residual mean circulation in the middle atmosphere for the northern winter period, *J. Atmos. Sci., 44*, 1437–1452, 1987.

Haberle, R. M., Interannual variability of global dust storms on Mars, *Science, 234*, 459–461, 1986.

Haberle, R. M., and B. M. Jakosky, Sublimation and transport of water from the north residual polar cap on Mars, *J. Geophys. Res., 95*, 1423–1437, 1990.

Haberle, R. M., and B. M. Jakosky, Atmospheric effects on the remote determination of thermalinertia on Mars, *Icarus, 90*, 187–204, 1991.

Haberle, R. M., C. B. Leovy, and J. B. Pollack, Some effects of global dust storms on the atmospheric circulation of Mars, *Icarus, 50*, 322–367, 1982.

Hamilton, K., and R. R. Garcia, Theory and observations of the short-period normal mode oscillations of the atmosphere, *J. Geophys. Res., 91*, 11,867–11,875, 1986.

Hanel, R., et al., Investigation of the Martian environment by infrared spectroscopy on Mariner 9, *Icarus, 17*, 423–442, 1972.

Hess, S. L., J. A. Ryan, J. E. Tillman, R. M. Henry, and C. B. Leovy, The annual cycle of pressure on Mars measured by Viking Landers 1 and 2, *Geophys. Res. Lett., 7*, 197–200, 1980.

Hitchman, M. H., and C. B. Leovy, Diurnal tide in the equatorial middle atmosphere as seen in LIMS temperatures, *J. Atmos. Sci., 43*, 557–561, 1985.

Houghton, J. T., and S. D. Smith, Remote sounding of atmospheric temperature from satellites, I, Introduction, *Proc. R. Soc. London Ser. A, 320*, 23–33, 1970.

Hunt, G. E., Thermal infrared properties of the Martian atmosphere, 4, Predictions of the presence of dust and ice clouds from Viking IRTM spectral measurements, *J. Geophys. Res., 84*, 2865–2874, 1979.

Jakosky, B. M., The role of seasonal reservoirs in the Mars water cycle, I, Seasonal exchange of water with the regolith, *Icarus, 55*, 1–18, 1983*a*.

Jakosky, B. M., The role of seasonal reservoirs in the Mars water cycle, II, Coupled models of the regolith, the polar caps, and atmospheric transport, *Icarus, 55*, 19–39, 1983*b*.

Jakosky, B. M., The seasonal cycle of water on Mars, *Space Sci. Rev., 41*, 131–200, 1985.

Jakosky, B. M., and E. S. Barker, Comparison of groundbased and Viking Orbiter measurements of Martian water vapor: Variability of the seasonal cycle, *Icarus, 57*, 322–334, 1984.

Jakosky, B. M., and C. B. Farmer, The seasonal and global behavior of water vapor in the Mars atmosphere: Complete global results of the Viking atmospheric water detector experiment, *J. Geophys. Res., 87*, 2999–3019, 1982.

Jakosky, B. M., and R. M. Haberle, The seasonal behavior of water on Mars, in *Mars*, edited by H. H. Kieffer et al., University of Arizona Press, in press, 1992.

James, P. B., The Martian hydrological cycle: Effects of CO_2 mass flux on global water distribution, *Icarus, 64*, 249–264, 1985.

James, P. B., and G. R. North, The seasonal CO2 cycle on Mars: An application of an energy balance climate model, *J. Geophys. Res., 87*, 10,271–10,283, 1982.

James, P. B., H. H. Kieffer, and D. A. Paige, The carbon dioxide cycle, in *Mars*, edited by H. H. Kieffer et al., University of Arizona Press, Tucson, in press, 1992.

Jaquin, F., P. Gierasch, and R. Kahn, The vertical structure of limb hazes in the Martian atmosphere, *Icarus, 68*, 442–461, 1986.

Justus, C. G., Mars global reference atmospheric model for mission planning and analysis, *J. Spacecr. Rockets, 28*, 216–221, 1991.

Kahn, R., Some observational constraints on the global-scale wind systems of Mars, *J. Geophys. Res., 88*, 10,189–10,209, 1983.

Kahn, R., The evolution of CO_2 on Mars, *Icarus, 62*, 175–190, 1985.

Kahn, R., Ice haze, snow, and the Mars water cycle, *J. Geophys. Res., 95*, 14,677–14,693, 1990.

Kahn, R., S. Lee, T. Z. Martin and R. Zurek, The Martian dust cycle, in *Mars*, edited by H. H. Kieffer et al., University of Arizona Press, Tucson, in press, 1992.

Kieffer, H. H., Mars south polar spring and summer temperatures: A residual CO_2 frost, *J. Geophys. Res., 84*, 8263–8288, 1979.

Leighton, R. B., and B. C. Murray, Behavior of carbon dioxide and other volatiles on Mars, *Science, 153*, 136–144, 1966.

Leovy, C. B., Observations of Martian tides over two annual cycles, *J. Atmos. Sci., 38*, 30–39, 1981.

Leovy, C. B., Martian meteorological variability, *Adv. Space Res., 2*, 19–44, 1982.

Leovy, C. B., The general circulation of Mars: Models and observations, *Adv. Geophys., 28*, 327–346, 1985.

Leovy, C. B., and Y. Mintz, Numerical simulation of the atmospheric circulation and climate of Mars, *J. Atmos. Sci., 26*, 1167–1190, 1969.

Leovy, C. B., R. W. Zurek, and J. B. Pollack, Mechanisms for Mars dust storms, *J. Atmos. Sci., 30*, 749–762, 1973.

Leovy, C. B., J. E. Tillman, W. R. Guest, and J. Barnes, Interannual variability of Martian weather, in *Recent Advances in Planetary Meteorology*, edited by G. Hunt, pp. 69–84, Cambridge University Press, New York, 1985.

Lindal, G. F., H. B. Hotz, D. N. Sweetnam, Z. Shippony, J. P. Brenkle, G. V. Hartsell, R. T. Spear, and W. H. Michael, Jr., Viking radio occultation measurements of the atmosphere and topography of Mars: Data acquired during 1 Martian year of tracking, *J. Geophys. Res., 84*, 8443–8456, 1979.

Lorenz, E. N., *The Nature and Theory of the General Circulation of the Atmosphere*, 162 pp., World Meteorological Organization, Geneva, 1967.

Martin, L. J., The major Martian yellow storm of 1971, *Icarus, 22*, 175–188, 1974*a*.

Martin, L. J., The major Martian dust storms of 1971 and 1973, *Icarus, 23*, 108–115, 1974*b*.

Martin, L. J., 1973 dust storm on Mars: Maps from hourly photographs, *Icarus, 29*, 363–380, 1976.

Martin, L. J., Clearing the Martian air: The troubled history of dust storms, *Icarus, 57*, 317–321, 1984.

Martin, L. J., and W. A. Baum, A study of cloud motions of Mars, final report B, JPL contract 951547, Lowell Observatory, Flagstaff, Ariz., 1969.

Martin, T. Z., Mean thermal and albedo behavior of the Mars surface and atmosphere over a Martian year, *Icarus, 45*, 427–446, 1981.

Martin, T. Z., Thermal infrared opacity of the Mars atmosphere, *Icarus, 66*, 2–21, 1986.

Martin, T. Z., A. R. Peterfreund, E. D. Miner, H. H. Kieffer, and G. E. Hunt, Thermal infrared properties of the Martian atmosphere, 1, Global behavior at 7, 9, 11, and 20 μm, *J. Geophys. Res., 84*, 2830–2842, 1979.

McCleese, D. J., et al., Remote sensing of the atmosphere of Mars using infrared pressure modulation and filter radiometry, *Appl. Opt.*, *25*, 4232–4245, 1986.

Moriyama, S., Effects of dust on radiation transfer in the martian atmosphere, III, Numerical experiments of radiative-convective equilibrium of the Martian atmosphere including the radiative effects due to dust, *J. Meteorol. Soc. Jpn.*, *54*, 52–57, 1976.

Moriyama, S., and T. Iwashima, A spectral model of the atmospheric general circulation of Mars: A numerical experiment including the effects of the suspended dust and the topography, *J. Geophys. Res.*, *85*, 2847–2860, 1980.

Murphy, J. R., O. B. Toon, R. M. Haberle, and J. B. Pollack, Numerical simulations of the decay of Martian global dust storms, *J. Geophys. Res.*, *95*, 14,629–14,648, 1990.

Paige, D. A., The annual heat balance of the Martian polar caps: Viking observations, Ph.D. thesis, 207 pp., Calif. Inst. of Technol., Pasadena, 1985.

Paige, D. A., and A. P. Ingersoll, Annual heat budget of martian polar caps: Viking Observations, *Science*, *228*, 1160–1168, 1985.

Paige, D. A., K. E. Herkenhoff, and B. C. Murray, Mariner 9 observations of the south polar cap of Mars: Evidence for residual CO_2 frost, *J. Geophys. Res.*, *95*, 1319–1335, 1990.

Palluconi, F. D., and H. H. Kieffer, Thermal inertia mapping of Mars from 60°S to 60°N, *Icarus*, *45*, 415–426, 1981.

Peterfreund, A. R., Contemporary aeolian processes on Mars: Local dust storms, Ph.D. thesis, 247 pp., Ariz. State Univ., Tempe, 1985.

Pirraglia, J., Martian atmospheric lee waves, *Icarus*, *7*, 517–530, 1976.

Pirraglia, J., and B. Conrath, Martian tidal pressure and wind fields obtained from the Mariner 9 infrared spectroscopy experiment, *J. Atmos. Sci.*, *31*, 318–329, 1974.

Pollack, J. B., Climatic change on the terrestrial planets, *Icarus*, *37*, 479–553, 1979.

Pollack, J. B., D. S. Colburn, F. M. Flasar, R. Kahn, C. E. Carlston, and D. Pidek, Properties and effects of dust particles suspended in the Martian atmosphere, *J. Geophys. Res.*, *84*, 2929–2945, 1979.

Pollack, J. B., C. B. Leovy, P. W. Greiman, and Y. Mintz, A Martian general circulation experiment with large topography, *J. Atmos. Sci.*, *38*, 3–29, 1981.

Pollack, J. B., J. F. Kasting, S. M. Richardson, and K. Poliakoff, The case for a wet, warm climate on early Mars, *Icarus*, *71*, 203–224, 1987.

Pollack, J. B., R. M. Haberle, J. Schaeffer, and H. Lee, Simulations of the general circulation of the Martian atmosphere, I, Polar processes, *J. Geophys. Res.*, *95*, 1447–1474, 1990.

Reber, C. A., The Upper Atmosphere Research Satellite, *Eos Trans. AGU*, *71*, 1867–1878, 1990.

Rodgers, C. D., Retrieval of atmospheric temperature and composition from remote measurements of thermal radiation, *Rev. Geophys. Space Phys.*, *14*, 609–624, 1976.

Ryan, J. A., Notes on the Martian yellow clouds, *J. Geophys. Res.*, *69*, 3759–3770, 1964.

Ryan, J. A., and R. M. Henry, Mars atmospheric phenomena during major dust storms, as measured at the surface, *J. Geophys. Res.*, *84*, 2929–2945, 1979.

Ryan, J. A., and R. D. Lucich, Possible dust devils, vortices on Mars, *J. Geophys. Res.*, *88*, 11,005–11,011, 1983.

Ryan, J. A., R. D. Sharman, and R. D. Lucich, Local Mars dust storm generation mechanism, *Geophys. Res. Lett.*, *8*, 899–901, 1981.

Salby, M. L., Sampling theory for asnoptic satellite observations, II, Fast Fourier synoptic mapping, *J. Atmos. Sci.*, *39*, 2601–2614, 1982*a*.

Salby, M. L., Sampling theory for asnoptic satellite observations, I, Space-time spectra, resolution, and aliasing, *J. Atmos. Sci.*, *39*, 2577–2600, 1982*b*.

Seiff, A., and D. B. Kirk, Structure of the atmosphere of Mars in summer at mid-latitudes, *J. Geophys. Res.*, *82*, 4364–4378, 1977.

Smith, A. K., and L. V. Lyjak, An observational estimate of gravity wave drag from the momentum balance in the middle atmosphere, *J. Geophys. Res.*, *90*, 2233–2241, 1985.

Taylor, F. W., Pressure modulator radiometry, *Spectrom. Tech.*, *4*, 137–197, 1983.

Thomas, P., and P. J. Gierasch, Dust devils on Mars, *Science*, *230*, 175–177, 1985.

Thorpe, T. E., Viking orbiter observations of atmospheric opacity during July-November 1976, *J. Geophys. Res.*, *82*, 4151–4159, 1977.

Tillman, J. E., Mars global atmospheric oscillations: Annually synchronized, transient normal mode oscillations and the triggering of global dust storms, *J. Geophys. Res.*, *93*, 9433–9451, 1988.

Toon, O. B., J. B. Pollack, and C. Sagan, Physical properties of the particles composing the Martian dust storm of 1971–1972, *Icarus*, *30*, 663–696, 1977.

Webster, P. J., The low-latitude circulation of Mars, *Icarus*, *30*, 626–649, 1977.

Zurek, R. W., Diurnal tide in the Martian atmosphere, *J. Atmos. Sci.*, *33*, 321–337, 1976.

Zurek, R. W., Solar heating of the Martian dusty atmosphere, *Icarus*, *35*, 196–208, 1978.

Zurek, R. W., Martian great dust storms: An update, *Icarus*, *50*, 288–310, 1982.

Zurek, R. W., Atmospheric tidal forcing of the zonal-mean circulation: The Martian dusty atmosphere, *J. Atmos. Sci.*, *43*, 652–670, 1986.

Zurek, R. W., Free and forced modes in the Martian atmosphere, *J. Geophys. Res.*, *93*, 9452–9462, 1988.

Zurek, R. W., and P. R. Christensen, Dust redistribution by east-west circulations on Mars (abstract), *Bull. Am. Astron. Soc.*, *22*, 1075, 1990.

Zurek, R. W., and C. B. Leovy, Thermal tides in the dusty Martian atmosphere: A verification of theory, *Science*, *213*, 437–439, 1981.

Zurek, R. W., and D. J. McCleese, The role of climate studies in the future exploration of Mars. The case for Mars III: Strategies for exploration—General interest and overview, edited by C. Stoker, *Sci. Technol. San Diego*, *74*, 277–285, 1989.

Zurek, R. W., J. R. Barnes, R. M. Haberle, J. B. Pollack, J. E. Tillman, and C. B. Leovy, Dynamics of the atmosphere of Mars, in *Mars*, edited by H. H. Kieffer, et al., University of Arizona Press, Tucson, in press, 1992.

R. D. Haskins, D. J. McCleese, J. T. Schofield, and R. W. Zurek, Earth and Space Sciences Division, Jet Propulsion Laboratory, California Institute of Technology, Pasadena, CA 91109.

C. B. Leovy, Department of Atmospheric Sciences, University of Washington, Seattle, WA 98195.

D. A. Paige, Department of Earth and Space Sciences, University of California, Los Angeles, CA 90024.

F. W. Taylor, Department of Atmospheric, Oceanic and Planetary Physics, Oxford University, Oxford OX1 3PU, England.

(Received May 6, 1991;
revised March 2, 1992;
accepted March 3, 1992.)